

## RESEARCH OUTPUTS / RÉSULTATS DE RECHERCHE

### Tracking developmentally regulated post-synthetic processing of homogalacturonan and chitin using reciprocal oligosaccharide probes

Mravec, Jozef; Kračun, Stjepan K.; Rydahl, Maja G.; Westereng, Bjørge; Miart, Fabien; Clausen, Mads H.; Fangel, Jonatan U.; Daugaard, Mathilde; Cutsem, Pierre Van; De Fine Licht, Henrik H.; Höfte, Herman; Malinovsky, Frederikke G.; Domozych, David S.; Willats, William G T

*Published in:*  
Development (Cambridge)

*DOI:*  
[10.1242/dev.113365](https://doi.org/10.1242/dev.113365)

*Publication date:*  
2014

*Document Version*  
Publisher's PDF, also known as Version of record

#### [Link to publication](#)

#### *Citation for pulished version (HARVARD):*

Mravec, J, Kračun, SK, Rydahl, MG, Westereng, B, Miart, F, Clausen, MH, Fangel, JU, Daugaard, M, Cutsem, PV, De Fine Licht, HH, Höfte, H, Malinovsky, FG, Domozych, DS & Willats, WGT 2014, 'Tracking developmentally regulated post-synthetic processing of homogalacturonan and chitin using reciprocal oligosaccharide probes', *Development (Cambridge)*, vol. 141, no. 24, pp. 4841-4850.  
<https://doi.org/10.1242/dev.113365>

#### General rights

Copyright and moral rights for the publications made accessible in the public portal are retained by the authors and/or other copyright owners and it is a condition of accessing publications that users recognise and abide by the legal requirements associated with these rights.

- Users may download and print one copy of any publication from the public portal for the purpose of private study or research.
- You may not further distribute the material or use it for any profit-making activity or commercial gain
- You may freely distribute the URL identifying the publication in the public portal ?

#### Take down policy

If you believe that this document breaches copyright please contact us providing details, and we will remove access to the work immediately and investigate your claim.

## RESEARCH ARTICLE

## TECHNIQUES AND RESOURCES

# Tracking developmentally regulated post-synthetic processing of homogalacturonan and chitin using reciprocal oligosaccharide probes

Jozef Mravec<sup>1,\*</sup>, Stjepan K. Kračun<sup>1,\*</sup>, Maja G. Rydahl<sup>1</sup>, Børge Westereng<sup>1,2</sup>, Fabien Miart<sup>3</sup>, Mads H. Clausen<sup>4</sup>, Jonatan U. Fangel<sup>1</sup>, Mathilde Daugaard<sup>4</sup>, Pierre Van Cutsem<sup>5</sup>, Henrik H. De Fine Licht<sup>1</sup>, Herman Höfte<sup>3</sup>, Frederikke G. Malinovsky<sup>1</sup>, David S. Domozych<sup>6</sup> and William G. T. Willats<sup>1,‡</sup>

## ABSTRACT

Polysaccharides are major components of extracellular matrices and are often extensively modified post-synthetically to suit local requirements and developmental programmes. However, our current understanding of the spatiotemporal dynamics and functional significance of these modifications is limited by a lack of suitable molecular tools. Here, we report the development of a novel non-immunological approach for producing highly selective reciprocal oligosaccharide-based probes for chitosan (the product of chitin deacetylation) and for demethylesterified homogalacturonan. Specific reciprocal binding is mediated by the unique stereochemical arrangement of oppositely charged amino and carboxy groups. Conjugation of oligosaccharides to fluorophores or gold nanoparticles enables direct and rapid imaging of homogalacturonan and chitosan with unprecedented precision in diverse plant, fungal and animal systems. We demonstrated their potential for providing new biological insights by using them to study homogalacturonan processing during *Arabidopsis thaliana* root cap development and by analyzing sites of chitosan deposition in fungal cell walls and arthropod exoskeletons.

**KEY WORDS:** Polysaccharides, *Arabidopsis*, Exoskeletons, Carbohydrate microarrays, Cell wall, Fluorescence imaging, Root cap

## INTRODUCTION

Many organisms produce polysaccharide-rich extracellular matrices, including the cell walls of plants and fungi, and the exoskeletons of arthropods. Homogalacturonan (HG) is a major structural feature of the pectic polysaccharides that are present in plant cell walls; it provides structural support, mediates cell adhesion, regulates wall porosity and generates a dynamic operating environment for other cell wall components (Caffall and Mohnen, 2009; Willats et al., 2001). HG is a linear polysaccharide composed of  $\alpha$ -(1→4)-linked D-galacturonic acid residues, which can be methyl esterified at C-6

(Caffall and Mohnen, 2009). HG is frequently subject to post-synthetic demethylesterification in the cell wall by pectin methylsterases (PMEs), and the degree of methyl esterification and the distribution of remaining ester groups profoundly impacts upon the functional properties of HG (Wolf et al., 2009). Plants typically produce dozens of PMEs, enabling them to fine-tune these functional properties *in muro* with exquisite precision within cell wall microdomains (Pelloux et al., 2007). The spatiotemporal regulation of PME activities is one of the key downstream components of many plant developmental pathways that determine growth and development, and responses to biotic and abiotic stresses (Wolf et al., 2009, 2012; Peaucelle et al., 2008; Peaucelle et al., 2011a; Peaucelle et al., 2011b; Ferrari et al., 2013).

Chitin, a polymer of  $\beta$ -(1→4)-linked *N*-acetylglucosamine is the main constituent of the exoskeletons of arthropods and of fungal cell walls, and may be deacetylated by chitin deacetylases (CDAs) to produce chitosan (Eijsink et al., 2010; Tsigos et al., 2000). Analogous to methyl esterification of HG, the degree of acetylation has important functional implications. In many cases, the biological significance of chitin acetylation state is poorly understood, but the quantity and ratio of chitin to chitosan is highly dynamic depending on the developmental phase and cellular interactions (Christodoulidou et al., 1999; Baker et al., 2011; Heustis et al., 2012; Luschign et al., 2006; Wang et al., 2006). For example, tracheal tube elongation in *Drosophila melanogaster* is regulated by luminal CDA proteins (Luschign et al., 2006; Wang et al., 2006).

Understanding the developmental roles and cellular processing of structural polysaccharides such as HG and chitosan requires specific detection of them *in situ* and, preferably, *in vivo*. Monoclonal antibodies (mAbs) and carbohydrate binding modules have been widely used as probes, but these large proteinaceous molecules have considerable limitations in terms of penetration and suitability for live- and real-time labelling (Verherbruggen et al., 2009; McCartney et al., 2006). Other advanced labelling procedures, such as the use of sugars attached *in vivo* through click chemistry, are powerful but time consuming and technically challenging (Anderson et al., 2012).

It is known that chitosan oligosaccharides (COS) can modulate the biological activity of oligogalacturonate (OGA) fragments of HG (Cabrera et al., 2010), and our molecular modelling of the COS and OGA interaction confirmed that their reciprocal binding is mediated by the precise alignment of the positively charged amino groups on COS and the negatively charged carboxyl groups on OGA (Fig. 1A). We exploited this natural affinity to develop oligosaccharide-based reciprocal probes for de-esterified HG and chitosan (Fig. 1B). These probes have several desirable features when compared with the use of antibodies: they are very rapid to use and easy to couple directly to a variety of tags; furthermore, their small size allows high-resolution

<sup>1</sup>Department of Plant and Environmental Sciences, University of Copenhagen, Frederiksberg 1871, Denmark. <sup>2</sup>Department of Chemistry, Biotechnology and Food Science, Norwegian University of Life Sciences, Aas NO-1432, Norway. <sup>3</sup>Institut Jean-Pierre Bourgin, UMR1318 INRA/AgroParisTech, Saclay Plant Sciences, INRA Centre de Versailles, Versailles 78026, Cedex, France. <sup>4</sup>Center for Nano medicine and Therapeutics and Department of Chemistry, Technical University of Denmark, Kongens Lyngby DK-2800, Denmark. <sup>5</sup>Unité de Recherche en Biologie cellulaire végétale, University of Namur, Namur B-5000, Belgium. <sup>6</sup>Department of Biology and Skidmore Microscopy Imaging Center, Skidmore College, Saratoga Springs, NY 12866, USA.

\*These authors contributed equally to this work

‡Author for correspondence (willats@plen.ku.dk)

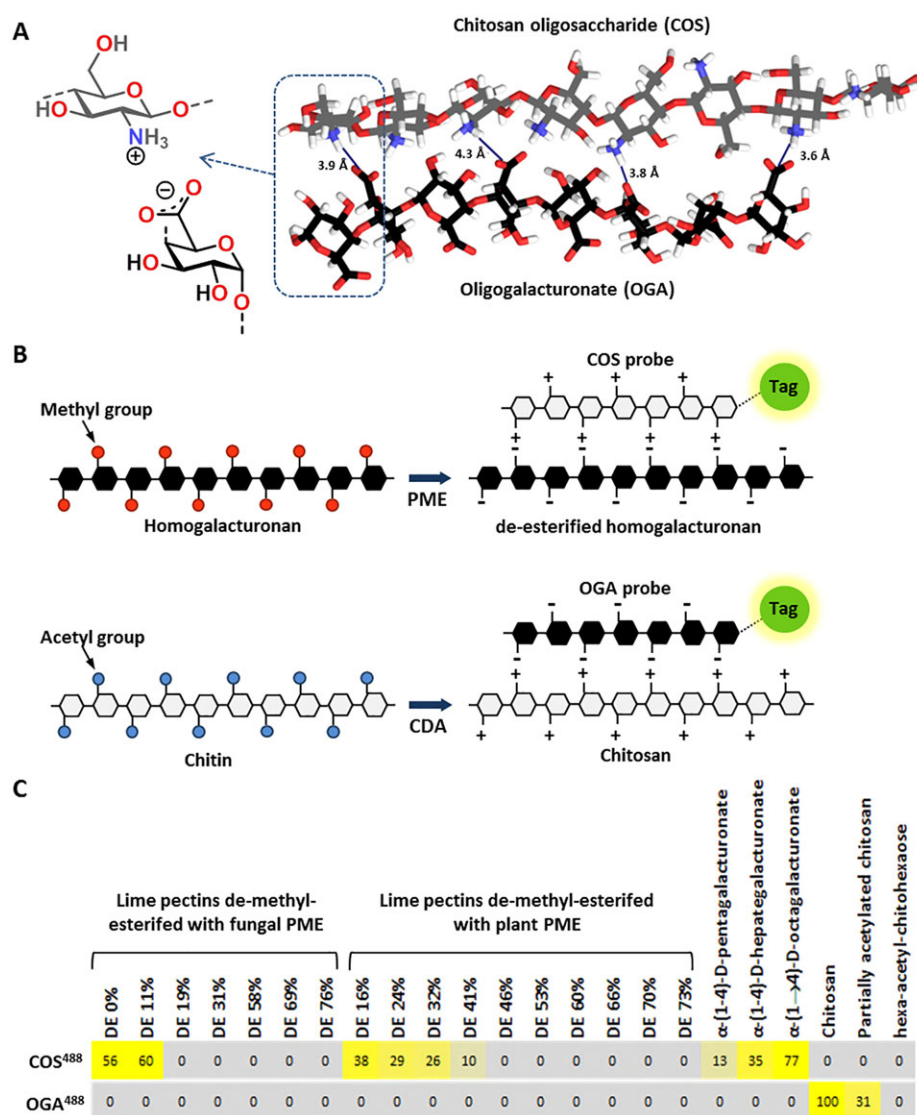


**Fig. 1. Reciprocal binding of oligogalacturonates and chitosan oligosaccharides.** (A) Molecular model showing the conformational features of oligogalacturonate (OGA) and chitosan oligosaccharides (COS) that promote binding by the alignment of opposing charges of the carboxyl groups on OGA and amino groups on COS. The numbers indicate the distance in Angstroms (Å) between carboxylate carbon atoms (on OGA) and ammonium group nitrogen atoms (on COS) after minimization. (B) Schematic showing the charge-based binding of COS and OGA to homogalacturonan (HG) with a low degree of methyl esterification (DE) and chitosan, respectively. Binding sites are created by pectin methyltransferases (PME) and chitin deacetylases (CDAs) acting on HG and chitin to form de-esterified HG and chitosan, respectively. Directly tagged COS and OGA probes were produced through coupling to a range of fluorophores or nanogold particles. The probes were named according to their tag; hence, a COS probe coupled to Alexa Fluor 488 is designated COS<sup>488</sup> and COS coupled to nanogold particles is COS<sup>AuNP</sup>. For MALDI-ToF analysis of COS and OGA, see supplementary material Fig. S1 and methods in the supplementary material. (C) The binding specificity of COS<sup>488</sup> and OGA<sup>488</sup> was tested by probing carbohydrate microarrays that were populated with the oligo- and polysaccharides listed, including lime pectins, with a range of degrees of methyl esterification. Numbers indicate normalized mean of spot signals obtained from microarrays. Colour intensity is correlated to signal strength. For more extensive specificity analysis and comparison with antibodies against HG, see supplementary material Fig. S2.

imaging and effective tissue penetration. Moreover, unlike antibodies, they are suitable for direct real-time imaging of polysaccharide processing.

## RESULTS

### Testing of COS<sup>488</sup> and OGA<sup>488</sup> reciprocal specificity using microarrays of defined glycans

COS and OGA samples (supplementary material Fig. S1) were coupled to aminoxy-functionalized Alexa Fluor fluorophores or to gold nanoparticles (Fig. 1B). To assess the binding specificities of these conjugates, we utilized carbohydrate microarrays (Pedersen et al., 2012) populated with 41 defined oligo- and polysaccharides. The arrays included pectin samples that had been treated with PMEs to produce HG with progressively lower degrees of methyl esterification. The COS probe coupled to Alexa Fluor 488 (COS<sup>488</sup>) bound to HG-containing pectic polysaccharides and to OGAs, but not to other oligo- or polysaccharides. Importantly, no binding to bovine serum albumin (BSA) or the polyanionic polysaccharides chondroitin sulphate A and B was observed (Fig. 1C; supplementary material Fig. S2). As expected, COS<sup>488</sup> binding to the pectic polysaccharides was positively correlated with decreasing degrees of methyl esterification, and to the oligosaccharides with increasing degrees of polymerization. In the case of oligosaccharides, the strongest binding was detected for

octagalacturonate, weaker binding for heptagalacturonate and pentagalacturonate, and no binding for shorter OGAs (Fig. 1C; supplementary material Fig. S2). Using the same approach, we also characterized the reciprocal probe, OGA coupled to Alexa Fluor 488 (OGA<sup>488</sup>). As predicted, this probe bound to chitosan and, more weakly, to partially acetylated chitosan but not to fully acetylated chitohexaose or any other oligo- or polysaccharides (Fig. 1C; supplementary material Fig. S2). These data indicate that COS and OGA are highly selective probes for non-methyl esterified HG and chitosan, respectively.

Only one antibody against chitosan has been reported (Sorlier et al., 2003), but several mAbs against HG have been described previously in detail (Verherbruggen et al., 2009), and we compared their binding to that of COS<sup>488</sup>. COS<sup>488</sup> binding was distinct from that of the seven mAbs against HG tested and was more selective towards sparsely methyl esterified pectins (supplementary material Fig. S2). It is worth noting that the mAb with the most similar binding profile to that of COS<sup>488</sup> was the synthetic phage display mAb PAM1, which is also produced non-immunologically (Willats et al., 1999). However, PAM1 binding, which requires at least 20 contiguous non-methyl esterified galacturonic acid residues, appears to be dependent on the helical conformation adopted by long stretches of non-esterified HG (Willats et al., 1999). This might account for the fact that PAM1 also



bound to DNA on arrays, whereas COS<sup>488</sup> binding to DNA was very weak (supplementary material Fig. S2).

### Detection of HG in diverse plant species using COS conjugates

We tested whether COS<sup>488</sup> could be used to directly visualize HG in a variety of plant systems (Fig. 2). Rapid (<20 min) labelling was possible by directly immersing the samples into a COS<sup>488</sup>-containing solution for a short time, followed by a brief washing step (Fig. 2A). HG-specific labelling was confirmed by using a set of controls that demonstrated the reduction of the labelling signal following treatment with polygalacturonase (supplementary material Fig. S3A–D). By using COS<sup>488</sup> in conjunction with mAb JIM7 (Verherbruggen et al., 2009), which recognizes highly methyl esterified HG, we were able to observe the cellular location of HG with different esterification states within discrete cell wall microdomains in *Arabidopsis* stem parenchyma cells (Fig. 2B–F). When initially synthesized and deposited in cell walls, HG typically had a high degree of methyl esterification, as shown by the labelling of JIM7 on the plasma membrane face of cell walls (Fig. 2B). Demethylesterified HG, produced by the activity of extracellular PME, is typically located between cells, where it is required for cell adhesion (Willats et al., 2001). Consistent with this, binding of COS<sup>488</sup> was restricted to the corners of intercellular spaces and middle lamellae (Fig. 2C,E,F). Using COS<sup>488</sup>, we also investigated the spatiotemporal distribution of HG in green algae, which often display highly dynamic HG post-synthetic modifications (Sørensen et al., 2011). In the charophyte alga *Micrasterias furcata*, at a late stage of cell division, COS<sup>488</sup> labelled punctate structures on the surface of the growing daughter semi-cell, but not the mother semi-cell (Fig. 2G). By contrast, the mother semi-cell, but not the daughter semi-cell was labelled with JIM7, which binds to HG that

has a high degree of methyl esterification (Fig. 2G). Labelling of whole cells of the multicellular *Spirogyra* sp. with COS<sup>488</sup> revealed demethylesterified HG that was present at the tips of growing cell outgrowths. Labelling was also strong at the junction planes between cells, and this is important because it suggests that the role of HG in cell adhesion emerged early in green plant evolution (Fig. 2H). The unicellular alga *Penium margaritaceum* is covered in a highly intricate pectin-rich lattice with projections (Fig. 2I). Labelling of *P. margaritaceum* demonstrated that the small size of the COS and OGA probes compared with that of antibodies (approximately 1.7 and >150 kDa, respectively) provided superior image resolution. Using COS<sup>488</sup>, this network was clearly resolved with particularly strong labelling of spine-like projections (Fig. 2J). Probing with the antibody JIM5 (against HG) produced a similar overall labelling pattern, but the resolution was apparently lower than that obtained using COS<sup>488</sup> (Fig. 2K). Moreover, using COS coupled to nanogold particles (COS<sup>AuNP</sup>) in conjunction with transmission electron microscopy enabled us to locate HG at the ultrastructural level (Fig. 2L; supplementary material Fig. S3E,F).

### The *Arabidopsis* root cap is a hotspot for HG de-esterification

The *Arabidopsis* root tip is a widely used developmental model in plant biology, and we analyzed HG distribution and turnover during root cap development using the COS probe (Fig. 3). As the outermost layer of the root cap matures with time, it is usually sloughed as a file of cells, sometimes called border-like cells. This is a cyclic event that protects the root proper during penetration through the soil (Bennett et al., 2010; Driouch et al., 2007; Fig. 3A,B). Many aspects of the cellular processes underlying root cap maturation, including cell wall turnover, are poorly understood, although a regulatory role for NAC transcription factors has been demonstrated previously (Bennett et al., 2010).

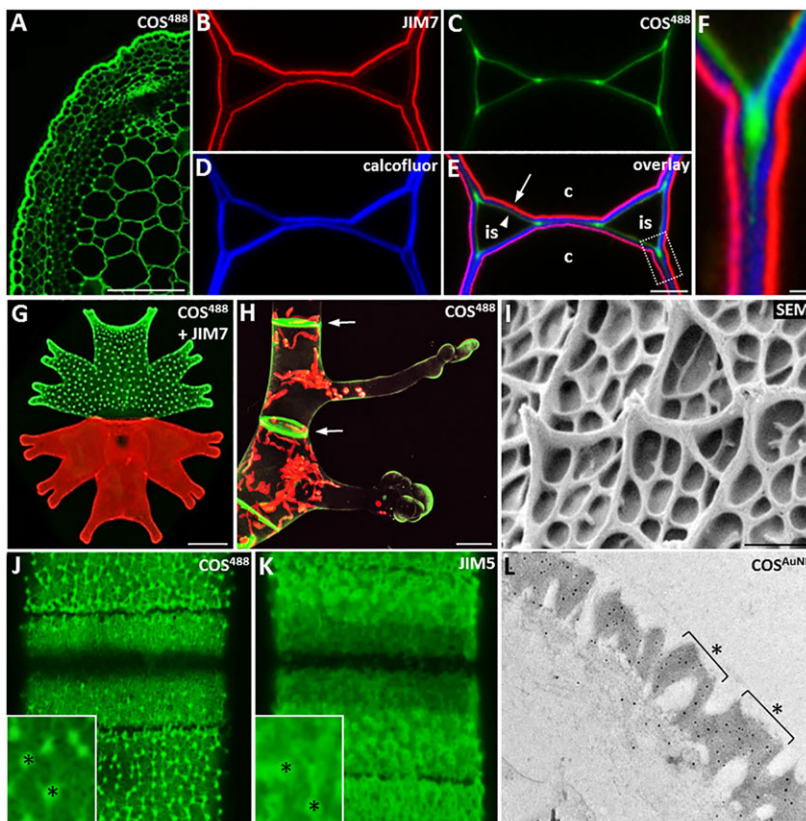


**Fig. 2. COS labelling of different plant species.**

(A) Labelling of homogalacturonan (HG) with COS<sup>488</sup> in a section through an *Arabidopsis* stem. (B–F) Triple labelling of *Arabidopsis* stem showing highly methyl esterified HG labelled with mAb JIM7 (B), de-esterified HG labelled with COS<sup>488</sup> (C) and cellulose labelled by using Calcofluor (D). (E) Overlay image showing COS<sup>488</sup> labelling the interface between cells (c) and intercellular spaces (is). The arrow indicates the position of the plasma membrane face of the wall, and the arrowhead denotes the middle lamella. (F) Higher magnification image of the intercellular space region (dashed box in E). (G) The alga *Micrasterias furcata* dual labelled with COS<sup>488</sup> (green) and the mAb JIM7 against HG (red). Note the developmentally regulated distribution of the highly methyl esterified HG that is recognized by JIM7 in the older mother cell (bottom) and the de-esterified HG recognized by COS<sup>488</sup> in the slightly smaller daughter cell (top). (H) Labelling of HG in *Spirogyra* sp. with COS<sup>488</sup> (green). Arrows indicate intercellular junction zones. Chloroplast auto-fluorescence is red. (I) Scanning electron micrograph (SEM) of the pectin-rich matrix on the surface of the unicellular alga *Penium margaritaceum*. (J,K) Fluorescent labelling of HG in the *P. margaritaceum* surface pectin matrix using COS<sup>488</sup> (J) and JIM5 (K). Insets show the close-up of the spine-like structures (asterisks). (L) Transmission electron microscopy showing the labelling of the *P. margaritaceum* outer pectic matrix (asterisks) using COS<sup>AuNP</sup> with silver enhancement. Scale bars: 100  $\mu$ m (A); 10  $\mu$ m (B–E,G,H,I,J,K); 1  $\mu$ m (F,I,L and J,K insets).

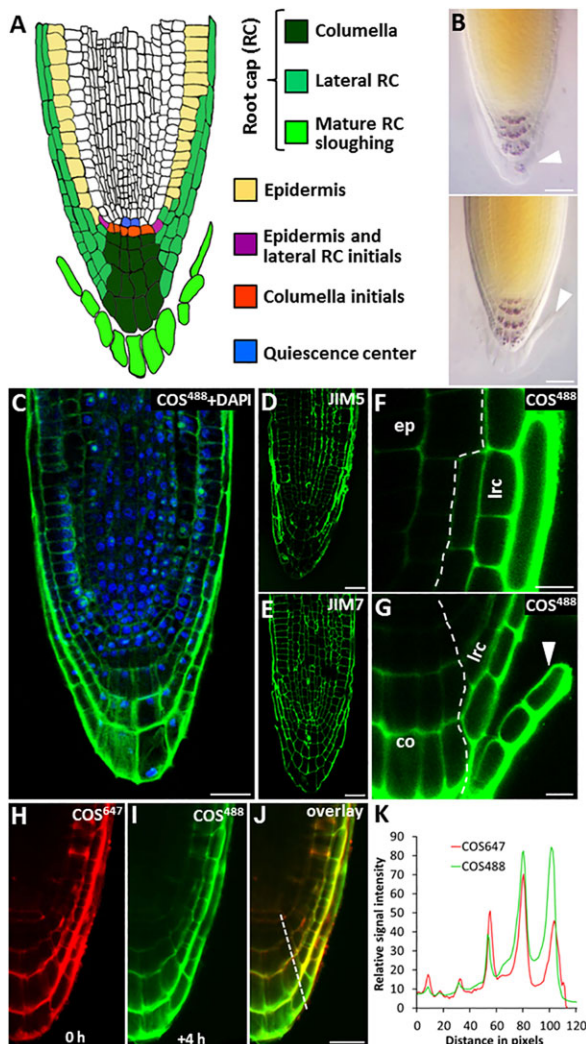


**Fig. 3. HG processing during root cap maturation in *Arabidopsis*.**

(A) Diagram showing the cellular anatomy of the *Arabidopsis* root tip with tissues related to the root cap (RC) highlighted. (B) Different phases of the mature root cap (arrowhead) sloughing. Top panel, the outermost layer of the root cap is mature and primed to be sloughed. Bottom panel, the sloughing usually begins from the lateral root cap region as one file of cells. (C) COS<sup>488</sup> (green) labelling of a thin longitudinal resin section through a root tip. Note the strong signal in the mature layer (outer-most layer of the root cap). DAPI (blue) was used to stain nuclei. (D,E) Labelling of resin sections by using mAbs against HG, JIM5 (D) and JIM7 (E). (F,G) Whole-mount labelling of the root tip using COS<sup>488</sup>. Note the labelling pattern is similar to that observed in resin sections. (F) The lateral root cap region and (G) the columella region. Note the sloughing cell layer (arrowhead). lrc, lateral root cap; ep, epidermis; co, columella. (H–K) Time-lapse experiment using two fluorescent variants of the COS probe. Seedlings were labelled first using COS<sup>647</sup> (red), washed and allowed to grow for 4 h. Seedlings were then re-labelled with COS<sup>488</sup> (green) and washed. The simultaneous scan of (H) COS<sup>647</sup> and (I) COS<sup>488</sup> labelling at the end of the experiment. (J) The overlay image shows the differences between the initial and the freshly formed HG with a low degree of methyl esterification. (K) Fluorescence plot profile of the two signals from H and I, the plot position is indicated as the dashed line in J. Note the higher accumulation of the COS<sup>488</sup> signal (freshly formed epitopes) in the cell walls of the mature layer of root cap than in the inner regions. This pattern was seen in 83% of cases (three independent experiments, at least eight roots were analyzed in each). Scale bars: 10  $\mu$ m.

The high penetrative capacity of COS<sup>488</sup> made it a promising tool in order to study the role of HG in this process, and when whole unfixed *Arabidopsis* roots were immersed in COS<sup>488</sup>, labelling was clearly observed at least three cell layers in from the epidermis. By

contrast, the mAbs JIM5 and JIM7 (Verhertbruggen et al., 2009) did not penetrate the epidermal cell layer (supplementary material Fig. S4A–D,G). We also produced longitudinal thin sections of resin-embedded root tips (Fig. 3C–E; supplementary material Fig. S4E,F). Labelling of these sections with COS<sup>488</sup> indicated that de-esterified HG appeared to be especially abundant in mature root cap cells (Fig. 3C). We also compared this pattern of staining with that of the mAbs JIM5 and JIM7. JIM5 labelling of HG was more pronounced in the mature lateral root cap but largely absent from the columella (Fig. 3D), whereas the JIM7 signal was uniformly distributed across the root tip with no obvious enrichment in the mature root cap layer (Fig. 3E). Because they are loosely attached, the mature root cap cells tend to be lost during resin embedding. By contrast, whole-mount *in vivo* labelling of intact root tips and then using COS<sup>488</sup> enabled observation of these cells during the process of detachment (Fig. 3F,G). It was notable that the cell walls of the root cap cells become thicker during maturation (supplementary material Fig. S4E–G). We measured the signal intensities of JIM5, JIM7 and COS<sup>488</sup> across the root tip and found that the signals increased for all three probes, but the increase was greater for JIM5 and COS<sup>488</sup> than that for JIM7. These observations indicated that the increased signals were not merely a function of greater wall thickness in mature root cells and that the occurrence of HG, especially with a lower degree of methyl esterification, was elevated in outer root cap cells (supplementary material Fig. S4E–G).

### Time-lapse labelling experiments to visualize HG dynamics in root cap

The root labelling experiments suggested that HG demethylesterification could be a distinctive feature of these cells related to their particular functional characteristics, and we further investigated this using a time-lapse experiment that exploited the live-labelling potential of the COS probes (Fig. 3H–J; supplementary material Fig. S5A–C). This experiment would not be feasible using mAbs because of the incompatibility between the conditions required for root growth and mAb binding. The basis of the experiment was to use two fluorescent variants of COS sequentially to distinguish original and newly generated HG epitopes within a relatively short time period (4 h). To accomplish this, we generated another fluorescent COS variant, conjugated to Alexa Fluor 647 (COS<sup>647</sup>), which had the same penetrative capacity and labelling pattern as COS<sup>488</sup> (supplementary material Fig. S5B,C). First, we labelled the seedlings with COS<sup>647</sup>, then washed out the probe and let them grow for 4 h, and then relabelled them with COS<sup>488</sup>. Initial labelling with COS<sup>647</sup> identified original demethylesterified HG (Fig. 3H), whereas the second labelling with COS<sup>488</sup> identified the demethylesterified HG that had freshly formed in the intervening 4 h period (Fig. 3I). The composite overlay image of the two labels indicated that the greatest abundance of newly formed demethylesterified HG was located in mature root cap cells (Fig. 3J,K). Importantly, the same result was also achieved in the reverse order, using first COS<sup>488</sup> and then COS<sup>647</sup>; therefore, this effect was not due to the different properties of the COS conjugates (supplementary material Fig. S5D–H).

### Several PME and PME-like genes are specifically expressed in the root cap

Because COS labelling experiments suggested a role for enhanced PME activity in root cap cells, we reviewed the expression profiles of PMEs and related genes in publically available microarray transcriptome databases. This showed that several PMEs and



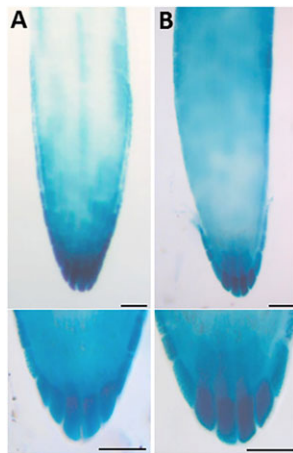


**Fig. 4. Expression of some PME related genes.** (A,B) GUS staining of reporter lines of root cap-specific PME-related genes. (A) Expression of PME-like gene At2g21610 and (B) PME-like gene At4g00080. The bottom panels show close-ups of the root cap regions. Note the higher expression in the maturing layer of the root cap. Scale bars: 10 µm.

PMEI enzymes exhibited strong and specific expression patterns in root cap cells (supplementary material Fig. S6). We confirmed this pattern for two PME- and PME-like genes by generating GUS reporter lines. Importantly, expression of both genes was upregulated in the mature layer of the root cap (Fig. 4A,B), suggesting that root cap maturation is indeed a hotspot of HG esterification processing through the activity of PMEs.

#### Consequences of the loss of COS<sup>488</sup> binding sites in mature root cap cells

We also investigated the physiological role of HG de-esterification in the root cap. We did not observe any phenotypic variation in the transfer (T)-DNA insertional mutants of the respective PME genes

compared with the phenotype of wild-type plants, and one probable explanation for this is the known high level of genetic redundancy of PMEs (Pelloux et al., 2007; Wolf et al., 2009). To overcome this, we employed a systemic chemical inhibitor of PMEs, (-)-epigallocatechin gallate (EGCG) (Lewis et al., 2008; Wolf et al., 2012), which targets PME activity *in vivo*. We treated seedlings with EGCG for 4 h at a concentration of 200 µM (this concentration did not completely inhibit root growth) or by directly supplementing EGCG to Murashige-Scoog agar plates at a concentration of 100 µM for continuous growth inhibition. Following treatment, the roots were labelled with COS<sup>488</sup>, JIM5 and JIM7, confirming that EGCG did indeed inhibit the formation of demethylesterified HG, whereas the highly methyl esterified HG was unchanged (Fig. 5A,B; supplementary material Fig. S5I). Inhibition during the pulse experiment was more pronounced than that upon continuous growth on EGCG, which further supports the notions that a feedback signalling loop exists (Wolf et al., 2012) and that the upregulation of some PMEs might partially diminish the inhibitory effect of EGCG (Fig. 5B). Next, we investigated the diminution of HG synthesis through COS<sup>488</sup> labelling of *quasimodo1* and *quasimodo2* mutants, which are defective in galacturonosyltransferase and methyltransferase activity, respectively (Bouton et al., 2002; Mouille et al., 2007). Both mutants have an HG content of approximately 50% of that in wild-type plants. Their characteristic phenotype is that of being defective in cell adhesion (Bouton et al., 2002; Mouille et al., 2007) with altered organization of border-like cells (Durand et al., 2009). The binding of COS<sup>488</sup> to both *quasimodo* mutant roots was substantially reduced, as was the case with treatment with EGCG (Fig. 5A,B), confirming that both HG synthesis and the activity of PME are responsible for the formation of COS<sup>488</sup>-binding epitopes.

The effect of EGCG on root cap physiology was further examined by growing seedlings on plates containing three concentrations of EGCG. We observed that treatment with EGCG resulted in the retention of root cap cells in a dose-dependent manner, such that

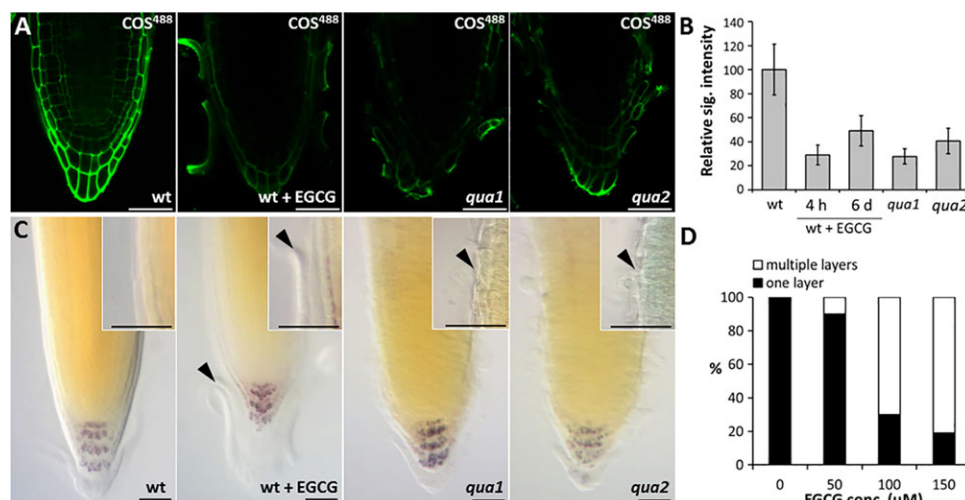


**Fig. 5. Functional analysis of COS epitopes in root cap.** (A,B) The effect of EGCG treatment and *quasimodo* mutations on the binding of COS<sup>488</sup> to *Arabidopsis* root tips. (A) Panels from left to right: wild type (wt), wild type continuously grown on 100 µM EGCG, *quasimodo1* (*qua1*) and *quasimodo2* (*qua2*) mutants. The COS<sup>488</sup> signal was reduced to similar degree in EGCG-treated roots and both *quasimodo* mutants. (B) Quantification of the COS<sup>488</sup> signals relative to that of wild type (the wild-type signal was set to 100%). The 4 h long pulse treatment with EGCG (200 µM) resulted in higher inhibition of the COS<sup>488</sup> signal than when roots were grown continuously for 6 days (6 d) on media supplemented with 100 µM EGCG. Error bars indicate s.e.m. ( $n=7$ ). (C,D) Phenotypes observed in the root tips grown on the EGCG and in the *quasimodo* mutants. Panels from left to right: wild type, wild type grown on 100 µM EGCG, *quasimodo1* and *quasimodo2* mutants. Insets are higher magnification images of the defects. Note the two layers of the mature root cap being detached in EGCG treated roots and premature detachment in *quasimodo* mutants. Defects are indicated by arrowheads. (D) Quantification of the effects on cell detachment of treatment with EGCG at different concentrations ( $n>20$ ). Scale bars: 10 µm.

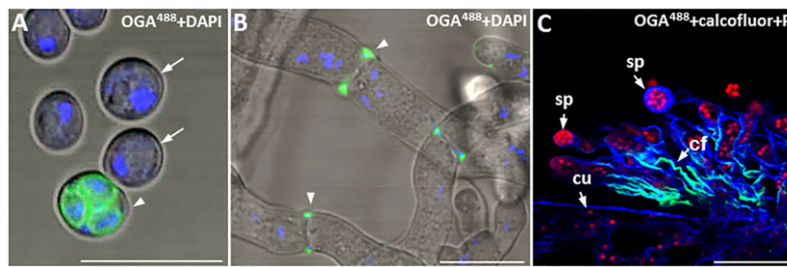


**Fig. 6. OGA labelling of different fungal species.** (A) OGA<sup>488</sup> labelling of chitosan (green) on the surface of a tetrad of four *Saccharomyces cerevisiae* spores (only three spores are visible). Note that the ascus wall (arrowhead) and diploid cells (arrows) are not labelled. Nuclei are stained by DAPI (blue). (B) *Neurospora crassa* mycelium labelled with OGA<sup>488</sup> (green). Chitosan is restricted to the septa between cells (arrowheads). Nuclei are stained by DAPI (blue). (C) Labelling of the chitosan by OGA<sup>488</sup> (green) in the pathogenic fungus *Entomophthora schizophorae* outgrowing housefly *Musca domestica*. Chitin is stained by Calcofluor (blue) and nuclei by propidium iodide (PI, red). Only conidiofores (cf) are labelled, but not spores (sp) or cuticle of the fly (cu). Scale bars: 10  $\mu$ m.

multiple layers of cells accumulated rather than being sloughed off (Fig. 5C,D). Interestingly, although *quasimodo* mutants and EGCG-treated plants both showed reduced binding of COS<sup>488</sup>, the effects on root cap cell separation were different. Although EGCG-treated plants exhibited root cap cell retention, this was not the case for the *quasimodo* mutants, in which we observed instances of premature separation (Fig. 5C). Thus, although reduced HG synthesis and the inhibition of PME activity are both characterized by the diminution of COS<sup>488</sup> epitopes, the physiological consequences are distinct. Taken together, these data provide new insights into the role of PMEs and HG turnover in root cap maturation, and demonstrate the potential of COS-based probes as powerful new tools for studying the developmental role of HG in plants.

#### Detection of chitosan in fungal cells using OGA<sup>488</sup>

Next, we tested whether the OGA-based probe OGA<sup>488</sup> could be used for chitosan detection in fungal model species (Fig. 6; supplementary material Fig. S7). *Saccharomyces cerevisiae* spores are known to have a cell wall structure that differs from that of diploid cells in that they possess a chitosan layer (Christodoulidou et al., 1999). Consistent with this, OGA<sup>488</sup> labelled the tetrad of spores inside asci, but did not label diploid cell walls (Fig. 6A). In another model fungi, *Neurospora crassa*, OGA<sup>488</sup> binding was restricted to septa between cells (Fig. 6B; supplementary material

Fig. S7A,B). Chitosan production has also been implicated in fungal pathogenesis (Baker et al., 2011), and we explored this in the context of host-parasite tissue interactions in the housefly *Musca domestica* that had been infected with the pathogenic fungus *Entomophthora schizophorae*. This fungus grows inside the fly haemocoel before corrupting host behaviour and inducing the fly to move to an elevated position where it attaches itself to the substrate and eventually dies (Roy et al., 2006). The fungus then grows out through the membrane between the sclerotized segments of the abdomen to produce new infectious spores. OGA<sup>488</sup> only labelled fungal structures and not fly tissue, and revealed that chitosan was exclusively located in the conidiophore cell walls emerging between the abdominal sclerites of the fly (Fig. 6C; supplementary material Fig. S7C-F).

#### OGA<sup>488</sup> as a tool to study the exoskeletons of arthropods

Finally, we used OGA<sup>488</sup> to probe for chitosan in arthropod species. Whole-mount labelling of adult *Drosophila* flies revealed that chitosan localized in the tarsal knee joints, with a higher abundance in the socket of the joint (Fig. 7A-D; supplementary material Fig. S8A-J). To confirm that this apparently restricted localization of chitosan was not simply owing to limited access in the whole-mount material, we also probed sections of resin-embedded material (supplementary material Fig. S8G-J). As expected, the leg exoskeleton was evenly labelled throughout by the chitin stain

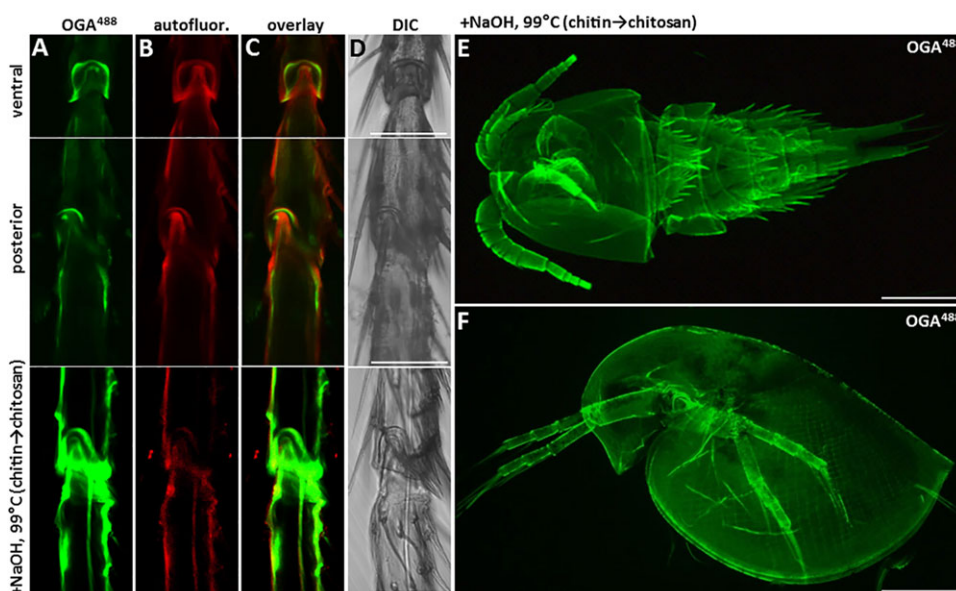


**Fig. 7. OGA labelling of exoskeletons of arthropods.** (A-D) OGA<sup>488</sup> labelling of *Drosophila* legs. Chitosan is restricted to the knee joint region with the most intense labelling in the socket. (A) OGA<sup>488</sup> labelling, (B) autofluorescence signal, (C) the overlay of signals from A and B. (D) Differential interference contrast (DIC) microscopy scan. Upper panels show the ventral view, middle and the bottom panels show the posterior view of the legs. The bottom panels show the OGA<sup>488</sup> labelling after treatment by NaOH to remove the acetyl groups. Note that the whole cuticle is now labelled. (E,F) OGA<sup>488</sup> labelling of exoskeletons of two small fresh water crustaceans that had been deacetylated using NaOH. (E) *Cyclops* sp. and (F) *Daphnia pulex*. Scale bars: 10  $\mu$ m (D), 100  $\mu$ m (E,F).

Calcofluor, whereas the OGA<sup>488</sup> signal was still restricted to tarsal knee joints. To further validate that the epitope recognized by OGA<sup>488</sup> was indeed chitosan, we treated some samples with chitosanase and some we re-acetylated using pyridine-acetic anhydride. In both cases, the binding of OGA<sup>488</sup> was greatly diminished (supplementary material Fig. S8E,F). Moreover, we also performed chemical deacetylation of all chitin that was present in the legs of *D. melanogaster* using concentrated NaOH (Kurita et al., 1991). This treatment converts chitin to chitosan, and as expected resulted in strong OGA<sup>488</sup> labelling in the whole leg cuticle (Fig. 7A–D, bottom panels). Thus, treatment with NaOH followed by OGA<sup>488</sup> labelling is an efficient way to detect chitin per se, and we demonstrated this approach on small fresh water crustaceans *Cyclops* sp. and *Daphnia pulex*, in which the majority of the exoskeleton is constructed of chitin (Fig. 7E–F; supplementary material Fig. S8K–Q). In *Cyclops* sp., chitosan only occurs in a region of the segmented body and in the tail appendages (supplementary material Fig. S8L). After NaOH deacetylation, OGA<sup>488</sup> labelled the entire exoskeleton (Fig. 7E; supplementary material Fig. S8N). Similarly, OGA<sup>488</sup> labelling of untreated *Daphnia pulex* exoskeletons showed only weak signals, but after deacetylation the whole specimen was brightly stained, which was again lost after chemical re-acetylation (Fig. 7F; supplementary material Fig. S8O–Q).

## DISCUSSION

By exploiting their unique physicochemical properties, we have developed a new class of molecular probes for HG, chitosan, and in combination with sodium hydroxide pre-treatment, also chitin. These new tools address significant analytical deficiencies and have several distinct advantages over antibodies: one-step labelling is rapid and simple, their small size ensures excellent tissue penetration and high resolution, and the ease of direct conjugation to a variety of tags facilitates dual labelling and time course experiments. An important additional feature is that, unlike antibodies, these probes are not optimized for use at the mammalian physiological pH of around 7. This is especially important in the case of plant research because most antibodies are not compatible with plant growth conditions (usually less than pH 5.7) and therefore cannot be used for live-labelling studies. This is a serious limitation because it means that HG localization studies have been largely confined to dead, sectioned plant materials without the possibility to investigate the often rapid and highly dynamic processes associated with HG synthesis and processing.

The epitope and paratope interactions that govern the binding of conventional hybridoma-based mAbs are generally mediated by a variety of non-covalent bonds, and this contribution from multiple forces might explain why relatively subtle variations in the degree of methyl esterification are not sufficient to define specificity in these mAbs. This is especially true for the most commonly used probe against HG, mAb JIM5, which binds to HG with a relatively broad range of degrees of methyl esterification (supplementary material Fig. S2). By contrast, because binding of COS and OGA probes appears to be entirely mediated by ionic interactions and particular molecular stereochemistry, they are highly sensitive to changes in methylation and acetylation status; thus, they are well suited to study chitin and HG synthesis, and subsequent processing by PME and CDAs.

The study of *Arabidopsis* root tips demonstrated the potential of the COS probe for tracking HG turnover *in vivo*. Our data indicated that, in *Arabidopsis* root cap cells, the inhibition of demethylesterification, as well as lower levels of HG synthesis,

resulted in a reduction of COS binding sites with some distinct cellular consequences. HG with a low degree of methyl esterification has been associated with the formation of Ca<sup>2+</sup>-crosslinked ‘egg box’ structures that are generally considered to promote cell-to-cell adhesion (Fig. 2C). Consistent with this, loss or reduction of HG synthesis leads to defects in cell adhesion, as seen in the *quasimodo* mutants (Bouton et al., 2002; Mouille et al., 2007). Conversely, removal of methyl esters also creates cleavage sites for certain HG-degrading enzymes, for example polygalacturonases, that act to disassemble HG networks and promote cell separation (Rhee et al., 2003; Francis et al., 2006; Ogawa et al., 2009). This might explain the reduced cell separation defect after PME inhibition by EGCG. However, the pectin degrading activity during separation should be apparent through the loss of the COS signal. In fact, we observed strong COS labelling before and after separation in mature root cap cells (Fig. 3F,G). One explanation for this intriguing finding is that in these cells, which are subjected to an unusual degree of mechanical stress, Ca<sup>2+</sup>-crosslinked HG plays a primary role in cell wall stiffening rather than adhesion. If Ca<sup>2+</sup>-crosslinked HG is used for this purpose, it might limit the formation of egg box structures that are available between the cells. Partial loss of PME activity would make more HG available in middle lamellae than usual and would explain the observed phenotypes in the EGCG-treated seedling. Taken together, our findings demonstrate that HG methylation is fine-tuned at the cellular level and provide evidence for a possible new and subtle aspect of this regulation operating in a subset of root cells.

OGA probes appear to be powerful new tools for studying chitosan deposition in opisthokonts, and we newly identify several instances of restricted chitosan production in model organisms. Additional genetic and physiological experiments would be necessary to fully understand the biological roles of chitosan, but some insight into functionality can be inferred from its known physicochemical properties (Rinaudo, 2006) and the localization experiments described here. For example, chitosan in the sporangiothecae of *E. schizophorae* might facilitate the hydration of the fungal tissue after exiting the host environment, and the chitosan in tarsal joints might play a role in lubrication. This notion is supported by the fact that silencing of a CDA gene in the beetle *Tribolium castaneum* results in impaired articulation of tibial-femoral joints in adult animals (Arakane et al., 2009).

In conclusion, we believe that OGA- and COS-based probes have the potential to shed new light on the numerous subtle and dynamic processes that are associated with chitin and HG post-synthetic developmental regulation. Because the properties that promote reciprocal binding are particular to COS and OGA, the potential for extending this general concept to other oligosaccharides could be limited. Nevertheless, the glycan microarrays we used for this study would be well suited to screening large chemical libraries, and new candidates might emerge using this approach.

## MATERIALS AND METHODS

### Sourcing and growth of plant, animal and fungal materials

*Penium margaritaceum*, *Micrasterias furcata* and *Spirogyra* sp. were grown in sterile liquid Woods Hole Medium (WHM) at 18°C under 2000 lux of cool white fluorescent light with a 16 h light:8 h dark photoperiod. Cells were collected by using centrifugation and then washed three times with WHM before labelling or experimental treatment. *Arabidopsis thaliana* Col-0, Ws, *qua1-2* (Bouton et al., 2002), *qua2-1* (Mouille et al., 2007) and tobacco plants were grown in a greenhouse (long day, 22°C). *Arabidopsis* seedlings were grown on vertical Murashige-Scoog plates with 1% sucrose in a growth chamber (long day, 21°C). To create the GUS reporter lines, the genomic



fragment of At2g21610, including 1385 bp of the promoter region, and the promoter region of At4g00080 (1385 bp upstream of ATG) were amplified and cloned into pGWB3 (Nakagawa et al., 2007) using Gateway technology (Invitrogen). The resulting constructs were transformed by using the *Agrobacterium*-mediated floral dip method to Col-0 plants. The GUS staining was performed as described previously (Benková et al., 2003). *Saccharomyces cerevisiae* strain BY4743 was cultivated on yeast peptone dextrose (YPD) plates, and the sporulation was performed as described previously (Elrod et al., 2009). *Neurospora crassa* FGSC no. 2489 was grown on potato dextrose agar plates. *Drosophila melanogaster* strain Oregon-R-S was cultivated in standard conditions on cornmeal media, anaesthetized with ether and fixed in 70% ethanol. *Cyclops* sp. was collected in a local pond and *Daphnia pulex* was obtained from a shop selling aquarium supplies. *Entomophthora schizophorae* was cultivated by consecutively infecting adult houseflies, *Musca domestica*, by placing sporulating fly cadavers over small plastic cups covered with insect netting and allowing spores to shoot downwards onto 20–30 flies. After an incubation period of 5–7 days at 21°C, dead flies attached to the underside of the net were collected for analysis.

### Arabidopsis physiological experiments

At 6 days of age, *Arabidopsis* seedlings were grown on vertical plates supplemented with or without EGCG (Sigma) from a 100 mM aqueous stock solution. The phenotypes were observed under a light microscope after Lugol staining and chloralhydrate clearing, as described previously (Benková et al., 2003). For the short term inhibitory experiments, seedlings were transferred from solid plates to liquid Murashige-Scoog that had been supplemented with 200 µM EGCG, and then incubated for 4 h, washed twice with MES buffer and probed with COS<sup>488</sup>.

### Molecular interaction modelling

The illustration of the oligosaccharides was generated using MacroModel (<http://schrodinger-macromodel-v99111.software.informer.com/9.9/>) using the fragment library. The conformational search was performed using MacroModel and the OPLS\_2005 force field. Water solvation was simulated implicitly by MacroModel. Charges were taken from the structure file. The conformational searches were carried out using 10,000 steps of the Monte Carlo multiple minimum (MCM) torsional sampling procedure and applying an energy window of 21 kJ/mol. No ring-opening or closing was allowed. The lowest energy conformations of COS and OGA from the minimizations were combined.

### Conjugation of COS and OGA with fluorescent tags

COS were prepared as previously described (Cabrera et al., 2010) and had a degree of polymerisation between 6 and 11. OGAs were prepared as described previously (van Alebeek et al., 2003), and OGA with a degree of polymerisation of 7 was used for preparation of the OGA probes. OGAs with degrees of polymerization from 3 to 8 were also produced and used on the microarray. The partially acetylated chitosan sample was produced as previously described (Kurita et al., 1991). Oligosaccharides, 10 mg/ml for COS and 1 mg/ml for OGA, were dissolved in 0.1 M NaOAc buffer, pH 4.9 and incubated with aminooxy-functionalized fluorophores Alexa Fluor 488 and Alexa Fluor 647 (Invitrogen) at 10 mg/ml in water at a ratio of 0.5 equivalents for the OGA probes and 0.1 equivalents for COS. The reaction mixture was incubated with shaking at 1400 r.p.m. in the dark at 37°C for 24 h and for a further 24 h at room temperature. The reaction mixtures were stored at –20°C in the dark and used without purification.

### Conjugation of COS with nanogold particles

A heterobifunctional aminooxy/amino linker was synthesized as described previously (Bohorov et al., 2006) and was reacted (1 mg, 1 equivalent) with 157 mg of COS (25 equivalents) at 37°C for 48 h with shaking at 1400 r.p.m. in 1 ml of 0.1 M NaOAc buffer, pH 4.9. The product was lyophilized and used without purification. 20 mg of the COS with the bi-functional linker was reacted with the mono-sulfo-NHS-Nanogold nanoparticle suspension (50 µl; Nanoprobe) together with 450 µl of 0.1 M potassium phosphate buffer, pH 8.0 and incubated at room temperature for 2 h with shaking at

1400 r.p.m. After that, 1 µl of ethanolamine was added to the mixture to block unreacted sulfo-NHS esters, and the reaction mixture was incubated for an extra 30 min. The nanoparticles were then purified by filtration through 10 kDa molecular mass cut-off filters (Nanosep 10 K Omega) and washed three times with 400 µl of water. The particles were then collected from the filter in 100 µl of water. Negative controls (ethanolamine<sup>AuNP</sup> and linker<sup>AuNP</sup>) were produced in an identical fashion by reacting the nanogold particles with ethanolamine (1 µl) or the linker (1 mg) under the same reaction conditions.

### Carbohydrate microarrays of oligo- and polysaccharides

Carbohydrate microarrays were produced, probed with antibodies and quantified as described previously (Pedersen et al., 2012). For probing with COS<sup>488</sup> and OGA<sup>488</sup> probes, the arrays were blocked with 5% skimmed milk in MES buffer pH 5.7 for 30 min followed by three washes with MES buffer. COS<sup>488</sup> or OGA<sup>488</sup> were applied to arrays for 15 min, diluted 1 in 1000 in MES buffer. After washing three times, each for 10 min, with MES buffer, the arrays were dried prior to scanning (GenePix 4400) and quantified as described previously (Pedersen et al., 2012).

### Transmission electron microscopy of *Penium margaritaceum* cell walls using COS<sup>AuNP</sup>

Centrifugation was used to collect 7-day-old cultures of *P. margaritaceum*, washed and spray-frozen in liquid propane as previously described (Domozych, 1999). The cells were then freeze substituted in 0.5% glutaraldehyde with acetone for 48 h at –80°C. The cells were warmed to –20°C, washed with cold acetone and then infiltrated and embedded in London Resin at –20°C. Polymerization was by UV light over 16 h at –20°C. Sections (50–70 nm) were obtained using a Leica Ultramicrotome and collected on formvar coated nickel grids. The sections were incubated for 2 h at room temperature or overnight at 4°C in either 1 µg/ml COS<sup>AuNP</sup> or ethanolamine<sup>AuNP</sup> and linker<sup>AuNP</sup>. The sections were then washed extensively with deionized water, fixed with 1% glutaraldehyde in PBS buffer for 3 min and washed over 5 min in deionized water. The sections were then treated with HQ silver enhancement solution (Nanoprobes) for 4 min and counterstained with 1% uranyl acetate for 5 min. The sections were viewed with a Zeiss Libra 120 transmission electron microscope at 120 kV.

### Chemical and enzymatic treatment

For deacetylation, samples were chemically deacetylated through pre-treatment with 5 M NaOH at 99°C for 1 h and extensively washed with water before labelling. For re-acetylation, samples were incubated with pyridine as a base catalyst for 20 min. The same amount of acetic anhydride was then added, and the mixture was incubated for 30 min. The samples were washed twice with 0.1 M sodium methoxide in methanol to remove O-acetyl groups while preserving N-acetyl groups, and the sample was then washed with water four times before staining. For chitosanase treatment, samples were incubated in 0.03 U/ml of chitosanase (Sigma) in 50 mM sodium acetate buffer (pH 5.0) overnight at 37°C. For polygalacturonase treatment, samples were incubated in endo-polygalacturonase (Megazyme) 2.5 U/ml in 100 mM sodium acetate buffer (pH 4.2) for 3 h at 37°C.

### Labelling of samples using fluorophore-conjugated COS and OGA

In all cases, COS<sup>488</sup>, COS<sup>647</sup> and OGA<sup>488</sup> were applied diluted 1 in 1000 in 50 mM MES pH 5.7. After 15 min, the samples were washed several times with MES buffer and mounted in MES buffer and glycerol solution (1:1) before viewing. Stem sections (100 µm thick) of *Arabidopsis* and tobacco were prepared using vibrating microtome (Vibratome, Leica VT1000S). Prior to sectioning, samples were embedded in 8% agarose gel. For COS<sup>488</sup> labelling of algal materials, algae were washed three times in WHM containing 9 mg/ml of MES, and the pH was adjusted to 5.7 with MES. The algae were then labelled in the dark at room temperature as described above. Where antibodies were used in conjunction with COS probes, resin sectioning and immunocytochemistry was performed as described previously (Sørensen et al., 2011). Algae were viewed with either an Olympus Fluoview 300 or

1200 confocal laser microscope. All other materials were viewed using a Leica SP-5 confocal laser microscope. The signal intensities were quantified by using ImageJ software.

### Competing interests

The authors declare no competing financial interests.

### Author contributions

J.M. developed the probes; S.K.K. synthesized the probes; M.G.R. generated binding data on carbohydrate arrays; B.W., F.M. and F.G.M. performed analytical and physiological experiments; P.V.C., H.H., H.H.D.F.L. and J.U.F. provided material and support; D.S.D. performed algal experiments; M.D. and M.H.C. performed the molecular modelling; W.G.T.W. designed the study and wrote the manuscript.

### Funding

This work was supported by the FP7 Marie Curie action project CeWalDyn under contract 329830 and Danish National Advanced Technology Foundation project B21st (J.M.); by the Danish Foundation for Strategic Research (S.K.K., M.H.C. and M.D.); by the Norwegian Research Council [214613]; by the FP7 project Waste2Go under contract 308363 (B.W.); and by the US National Science Foundation (NSF) Molecular and Cellular Bioscience [0919925] and NSF Division of Biological Infrastructure [0922805] (D.S.D.).

### Supplementary material

Supplementary material available online at  
http://dev.biologists.org/lookup/suppl/doi:10.1242/dev.113365/-DC1

### References

- Anderson, C. T., Wallace, I. S. and Somerville, C. R. (2012). Metabolic click-labeling with a fucose analog reveals pectin delivery, architecture, and dynamics in Arabidopsis cell walls. *Proc. Natl. Acad. Sci. USA* **109**, 1329–1334.
- Arakane, Y., Dixit, R., Begum, K., Park, Y., Specht, C. A., Merzendorfer, H., Kramer, K. J., Muthukrishnan, S. and Beeman, R. W. (2009). Analysis of functions of the chitin deacetylase gene family in *Tribolium castaneum*. *Insect Biochem. Mol. Biol.* **39**, 355–365.
- Baker, L. G., Specht, C. A. and Lodge, J. K. (2011). Cell wall chitosan is necessary for virulence in the opportunistic pathogen *Cryptococcus neoformans*. *Eukaryot. Cell* **10**, 1264–1268.
- Benková, E., Michniewicz, M., Sauer, M., Teichmann, T., Seifertová, D., Jürgens, G. and Friml, J. (2003). Local, efflux-dependent auxin gradients as a common module for plant organ formation. *Cell* **115**, 591–602.
- Bennett, T., van den Toorn, A., Sanchez-Perez, G. F., Campilho, A., Willemsen, V., Snel, B. and Scheres, B. (2010). SOMBRERO, BEARSKIN1, and BEARSKIN2 regulate root cap maturation in Arabidopsis. *Plant Cell* **22**, 640–654.
- Bohorov, O., Andersson-Sand, H., Hoffmann, J. and Blixt, O. (2006). Arraying glycomics: a novel bi-functional spacer for one-step microscale derivatization of free reducing glycans. *Glycobiology* **16**, 21C–27C.
- Bouton, S., Leboeuf, E., Mouille, G., Leydecker, M.-T., Talbot, J., Granier, F., Lahaye, M., Höfte, H. and Truong, H.-N. (2002). QUASIMODO1 encodes a putative membrane-bound glycosyltransferase required for normal pectin synthesis and cell adhesion in Arabidopsis. *Plant Cell* **14**, 2577–2590.
- Cabrera, J. C., Boland, A., Cambier, P., Frettinger, P. and Van Cutsem, P. (2010). Chitosan oligosaccharides modulate the supramolecular conformation and the biological activity of oligogalacturonides in Arabidopsis. *Glycobiology* **20**, 775–786.
- Caffall, K. H. and Mohnen, D. (2009). The structure, function, and biosynthesis of plant cell wall pectic polysaccharides. *Carbohydr. Res.* **344**, 1879–1900.
- Christodoulidou, A., Briza, P., Ellinger, A. and Bouriotis, V. (1999). Yeast ascospore wall assembly requires two chitin deacetylase isozymes. *FEBS Lett.* **460**, 275–279.
- Domozych, D. S. (1999). Disruption of the Golgi apparatus and secretory mechanism in the desmid, *Closterium acerosum*, by brefeldin A. *J. Exp. Bot.* **50**, 1323–1330.
- Drriouch, A., Durand, C. and Vitré-Gibouin, M. (2007). Formation and separation of root border cells. *Trends Plant Sci.* **12**, 14–19.
- Durand, C., Vitré-Gibouin, M., Follet-Gueye, M. L., Duponchel, L., Moreau, M., Lerouge, P. and Drriouch, A. (2009). The organization pattern of root border-like cells of Arabidopsis is dependent on cell wall homogalacturonan. *Plant Physiol.* **150**, 1411–1421.
- Eijsink, V. G. H., Hoell, I. A. and Vaaje-Kolstad, G. (2010). Structure and function of enzymes acting on chitin and chitosan. *Biotechnol. Genet. Eng. Rev.* **27**, 331–366.
- Elrod, S. L., Chen, S. M., Schwartz, K. and Shuster, E. O. (2009). Optimizing sporulation conditions for different *Saccharomyces cerevisiae* strain backgrounds. *Methods Mol. Biol.* **557**, 21–26.
- Ferrari, S., Savatin, D. V., Sicilia, F., Gramegna, G., Cervone, F. and Lorenzo, G. D. (2013). Oligogalacturonides: plant damage-associated molecular patterns and regulators of growth and development. *Front. Plant Sci.* **13**, 44–49.
- Francis, K. E., Lam, S. Y. and Copenhaver, G. P. (2006). Separation of Arabidopsis pollen tetrads is regulated by QUARTET1, a pectin methylesterase gene. *Plant Physiol.* **142**, 1004–1013.
- Heustis, R. J., Ng, H. K., Brand, K. J., Rogers, M. C., Le, L. T., Specht, C. A. and Fuhrman, J. A. (2012). Pharyngeal polysaccharide deacetylases affect development in the nematode *C. elegans* and deacetylate chitin in vitro. *PLoS ONE* **7**, e40426.
- Kurita, K., Kamiya, M. and Nishimura, S.-I. (1991). Solubilization of a rigid polysaccharide: controlled partial N-acetylation of chitosan to develop solubility. *Carbohydr. Polym.* **16**, 83–92.
- Lewis, K. C., Selzer, T., Shahar, C., Udi, Y., Tworowski, D. and Sagi, I. (2008). Inhibition of pectin methyl esterase activity by green tea catechins. *Phytochemistry* **69**, 2586–2592.
- Luschnig, S., Bätz, T., Armbruster, K. and Krasnow, M. A. (2006). serpentine and vermiform encode matrix proteins with chitin binding and deacetylation domains that limit tracheal tube length in *Drosophila*. *Curr. Biol.* **16**, 186–194.
- McCartney, L., Blake, A. W., Flint, J., Bolam, D. N., Boraston, A. B., Gilbert, H. J. and Knox, J. P. (2006). Differential recognition of plant cell walls by microbial xylan-specific carbohydrate-binding modules. *Proc. Natl. Acad. Sci. USA* **103**, 4765–4770.
- Mouille, G., Ralet, M.-C., Cavelier, C., Eland, C., Effroy, D., Hématy, K., McCartney, L., Truong, H. N., Gaudon, V., Thibault, J.-F. et al. (2007). Homogalacturonan synthesis in Arabidopsis thaliana requires a Golgi-localized protein with a putative methyltransferase domain. *Plant J.* **50**, 605–614.
- Nakagawa, T., Kurose, T., Hino, T., Tanaka, K., Kawamukai, M., Niwa, Y., Toyooka, K., Matsuoka, K., Jinbo, T. and Kimura, T. (2007). Development of series of gateway binary vectors, pGWBs, for realizing efficient construction of fusion genes for plant transformation. *J. Biosci. Bioeng.* **104**, 34–41.
- Ogawa, M., Kay, P., Wilson, S. and Swain, S. M. (2009). ARABIDOPSIS DEHISCENCE ZONE POLYGALACTURONASE1 (ADPG1), ADPG2, and QUARTET2 are Polygalacturonases required for cell separation during reproductive development in Arabidopsis. *Plant Cell* **21**, 216–233.
- Peaucelle, A., Louvet, R., Johansen, J. N., Höfte, H., Laufs, P., Pelloux, J. and Mouille, G. (2008). Arabidopsis phyllotaxis is controlled by the methyl-esterification status of cell-wall pectins. *Curr. Biol.* **18**, 1943–1948.
- Peaucelle, A., Braybrook, S. A., Le Guillou, L., Bron, E., Kuhlmeier, C. and Höfte, H. (2011a). Pectin-induced changes in cell wall mechanics underlie organ initiation in Arabidopsis. *Curr. Biol.* **21**, 1720–1726.
- Peaucelle, A., Louvet, R., Johansen, J. N., Salsac, F., Morin, H., Fournet, F., Belcram, K., Gillet, F., Höfte, H., Laufs, P. et al. (2011b). The transcription factor BELLRINGER modulates phyllotaxis by regulating the expression of a pectin methylesterase in Arabidopsis. *Development* **138**, 4733–4741.
- Pedersen, H. L., Fangel, J. U., McCleary, B., Ruzanski, C., Rydahl, M. G., Ralet, M.-C., Farkas, V., von Schantz, L., Marcus, S. E., Andersen, M. C. F. et al. (2012). Versatile high resolution oligosaccharide microarrays for plant glycobiology and cell wall research. *J. Biol. Chem.* **287**, 39429–39438.
- Pelloux, J., Rustérucchi, C. and Mellerowicz, E. J. (2007). New insights into pectin methylesterase structure and function. *Trends Plant Sci.* **12**, 267–277.
- Rhee, S. Y., Osborne, E., Poindexter, P. D. and Somerville, C. R. (2003). Microspore separation in the quartet 3 mutants of Arabidopsis is impaired by a defect in a developmentally regulated polygalacturonase required for pollen mother cell wall degradation. *Plant Physiol.* **133**, 1170–1180.
- Rinaudo, M. (2006). Chitin and chitosan: properties and applications. *Prog. Polym. Sci.* **31**, 603–632.
- Roy, H. E., Steinkraus, D. C., Eilenberg, J., Hajek, A. E. and Pell, J. K. (2006). Bizarre interactions and endgames: entomopathogenic fungi and their arthropod hosts. *Annu. Rev. Entomol.* **51**, 331–357.
- Sørensen, I., Pettolino, F. A., Bacic, A., Ralph, J., Lu, F., O'Neill, M. A., Fei, Z., Rose, J. K. C., Domozych, D. S. and Willats, W. G. T. (2011). The charophyte green alga provide insights into the early origins of plant cell walls. *Plant J.* **68**, 201–211.
- Sorlier, P., Hartmann, D. J., Denuzière, A., Viton, C. and Domard, A. (2003). Preparation and development of anti-chitosan antibodies. *J. Biomed. Mater. Res.* **A** **67**, 766–774.
- Tsigos, I., Martinou, A., Kafetzopoulos, D. and Bouriotis, V. (2000). Chitin deacetylases: new, versatile tools in biotechnology. *Trends Biotechnol.* **18**, 305–312.
- van Alebeek, G.-J. W. M., van Scherpenzeel, K., Beldman, G., Schols, H. A. and Voragen, A. G. J. (2003). Partially esterified oligogalacturonides are the preferred substrates for pectin methylesterase of *Aspergillus niger*. *Biochem. J.* **372**, 211–218.
- Verherbruggen, Y., Marcus, S. E., Haeger, A., Ordaz-Ortiz, J. J. and Knox, J. P. (2009). An extended set of monoclonal antibodies to pectic homogalacturonan. *Carbohydr. Res.* **344**, 1858–1862.
- Wang, S., Jayaram, S. A., Hemphälä, J., Senti, K.-A., Tsarouhas, V., Jin, H. and Samakovlis, C. (2006). Septate-junction-dependent luminal deposition of chitin deacetylases restricts tube elongation in the *Drosophila* trachea. *Curr. Biol.* **16**, 180–185.

- Willats, W. G. T., Gilmartin, P. M., Mikkelsen, J. D. and Knox, J. P.** (1999). Cell wall antibodies without immunization: generation and use of de-esterified homogalacturonan block-specific antibodies from a naive phage display library. *Plant J.* **18**, 57-65.
- Willats, W. G. T., Orfila, C., Limberg, G., Buchholt, H. C., van Alebeek, G. J., Voragen, A. G., Marcus, S. E., Christensen, T. M., Mikkelsen, J. D., Murray, B. S. et al.** (2001). Modulation of the degree and pattern of methyl-esterification of pectic homogalacturonan in plant cell walls. Implications for pectin methyl esterase action, matrix properties, and cell adhesion. *J Biol. Chem.* **276**, 19404-19413.
- Wolf, S., Mouille, G. and Pelloux, J.** (2009). Homogalacturonan methyl-esterification and plant development. *Mol. Plant.* **2**, 851-860.
- Wolf, S., Mravec, J., Greiner, S., Mouille, G. and Höfte, H.** (2012). Plant cell wall homeostasis is mediated by brassinosteroid feedback signaling. *Curr. Biol.* **22**, 1732-1737.



## **Supplementary Material and Methods**

### **MALDI-TOF-MS**

2  $\mu$ L of a 9 mg/mL mixture of 2,5-dihydroxybenzoic acid (DHB) in 30% acetonitrile was applied to a MTP 384-spot ground steel target plate TF (Bruker Daltonics). A 1  $\mu$ L sample was then mixed into the DHB droplet and dried under a stream of air. The samples were analysed with an Ultraflex MALDI-ToF/ToF instrument (Bruker Daltonics GmbH, Bremen, Germany) equipped with a nitrogen 337 nm laser beam. The instrument was operated in positive acquisition mode and controlled by the FlexControl 3.0 software package. All spectra were obtained using the reflectron mode with an acceleration voltage of 25kV, a reflector voltage of 26kV, and pulsed ion extraction of 40 ns in the positive ion mode. The acquisition range used was from  $m/z$  0 to 4000. The data was collected from averaging 1000 laser shots, with the lowest laser energy necessary to obtain sufficient signal to noise ratios. Peak lists were generated from the MS spectra using Bruker FlexAnalysis software (Version 3.3).

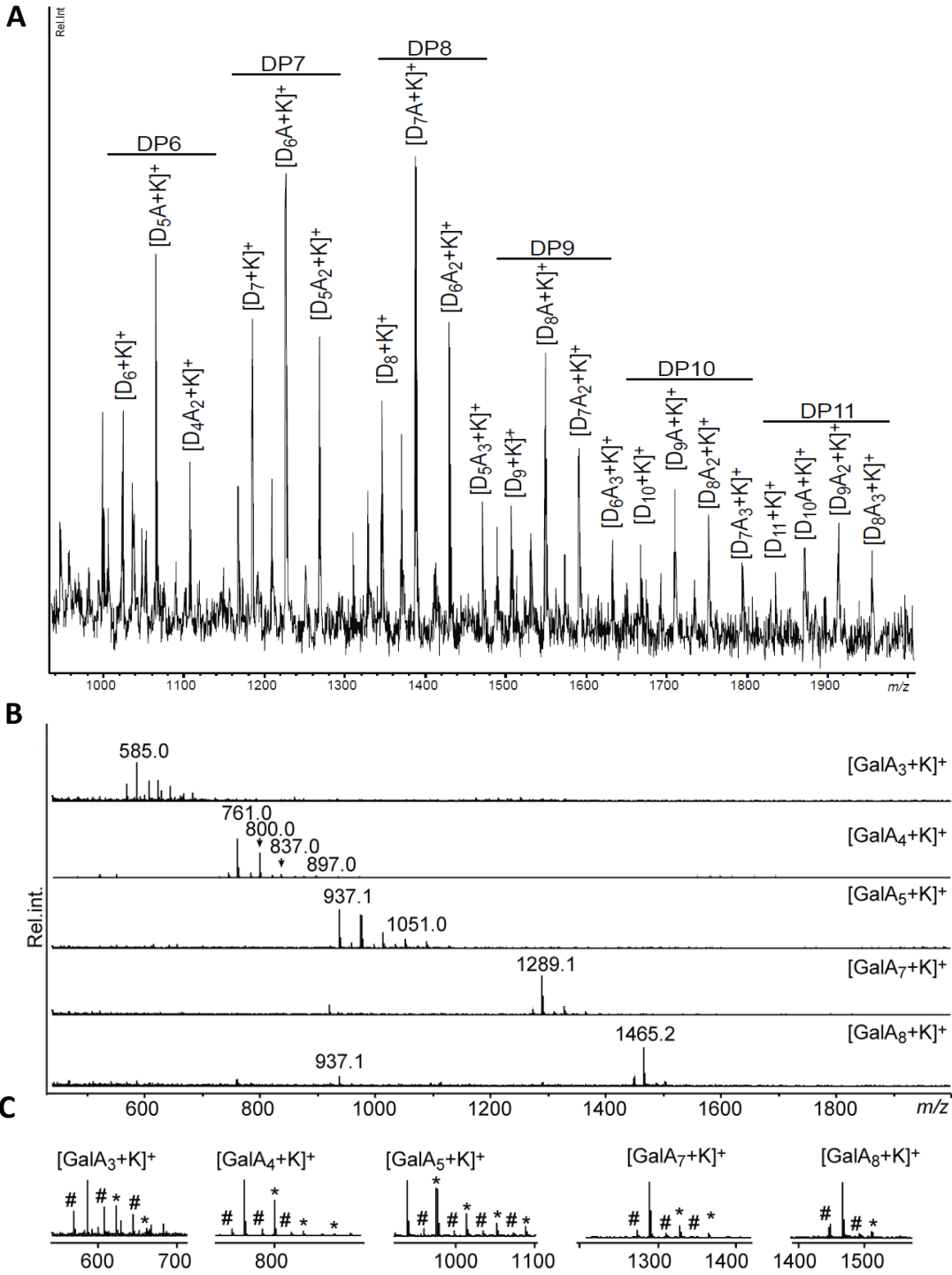


**Fig. S1. Oligosaccharide analysis using MALDI-ToF-MS.** (A) MALDI-ToF-MS spectrum of the chitosan oligosaccharides used to produce the COS probes.  $D_n$  is the degree of polymerisation and  $A_n$  is the number N-acetyl substitutions (B) MALDI-ToF-MS spectra of oligogalacturonides used on the microarrays and, in the case of GalA7, used to produce OGA probes. (C) Mass spectrum fragments showing sodium (hash) and potassium (asterisk) adducts from the spectrum shown in (B).

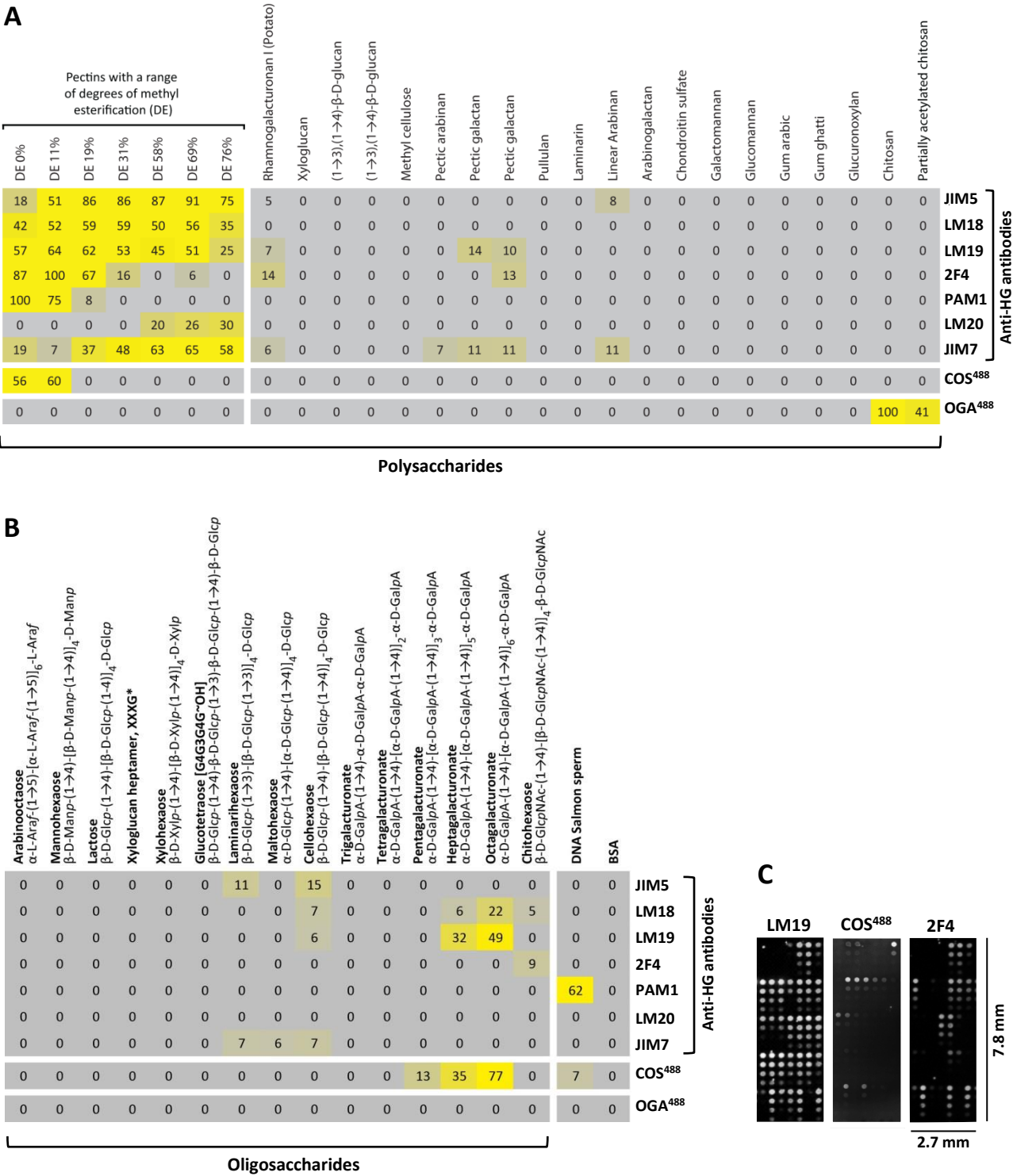


**Fig. S2. Binding specificity of COS and OGA.** Carbohydrate microarrays populated with (A) polysaccharides and (B) oligosaccharides were probed with a selection of anti-homogalacturonan antibodies (listed to the right), COS<sup>488</sup> and OGA<sup>488</sup>. The heatmap shows mean signal intensities from three replicate arrays. The highest signal in the data set was set to 100 and all other values adjusted accordingly. (C) Representative examples of carbohydrate microarrays from which the heatmap was produced.



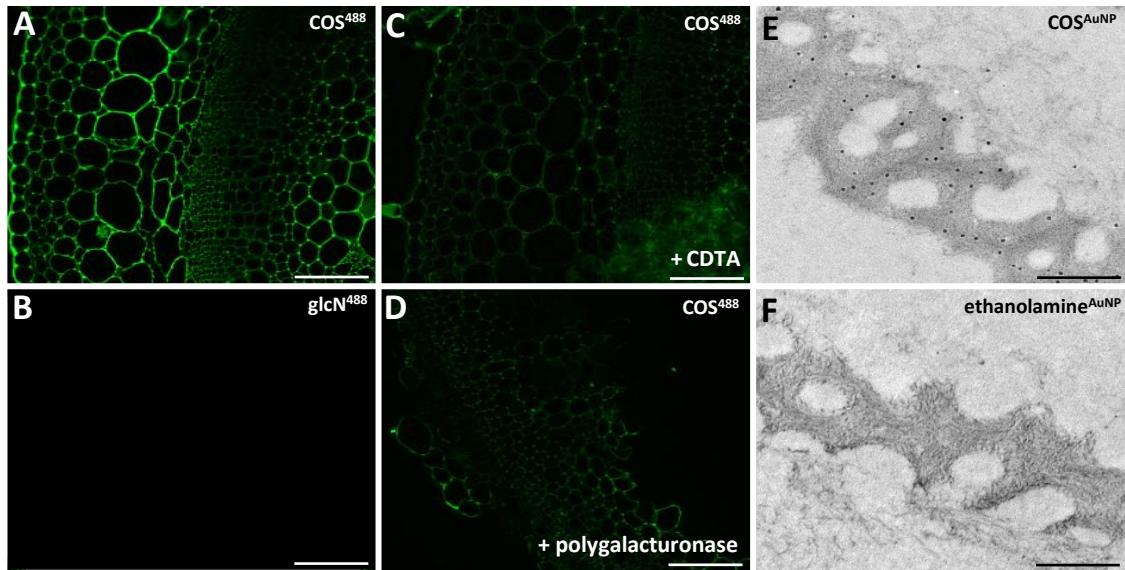


**Fig. S3. Microscopy labelling controls for COS binding.** (A-D) Sections through tobacco stem labelled with COS<sup>488</sup> (A) and control conjugate glucosamine<sup>488</sup> (B). Glucosamine was coupled to Alexa Fluor 488 using the same procedure as for COS<sup>488</sup>. Binding of COS<sup>488</sup> to tobacco sections was reduced by pre-treatment with a reagent used to extract pectins 1,2-cyclohexanediaminetetraacetic acid (C) and the homogalacturonan-degrading enzyme polygalacturonase (D). (E) Transmission electron microscopy images showing resin-embedded sections of *P. margaritaceum* labelled with COS coupled with nanogold particles (COS<sup>AuNP</sup>) and enhanced with silver. (F) A control image showing labelling with ethanolamine<sup>AuNP</sup>. Scale bars: 100 μm for A-D; 1 μm for E,F.

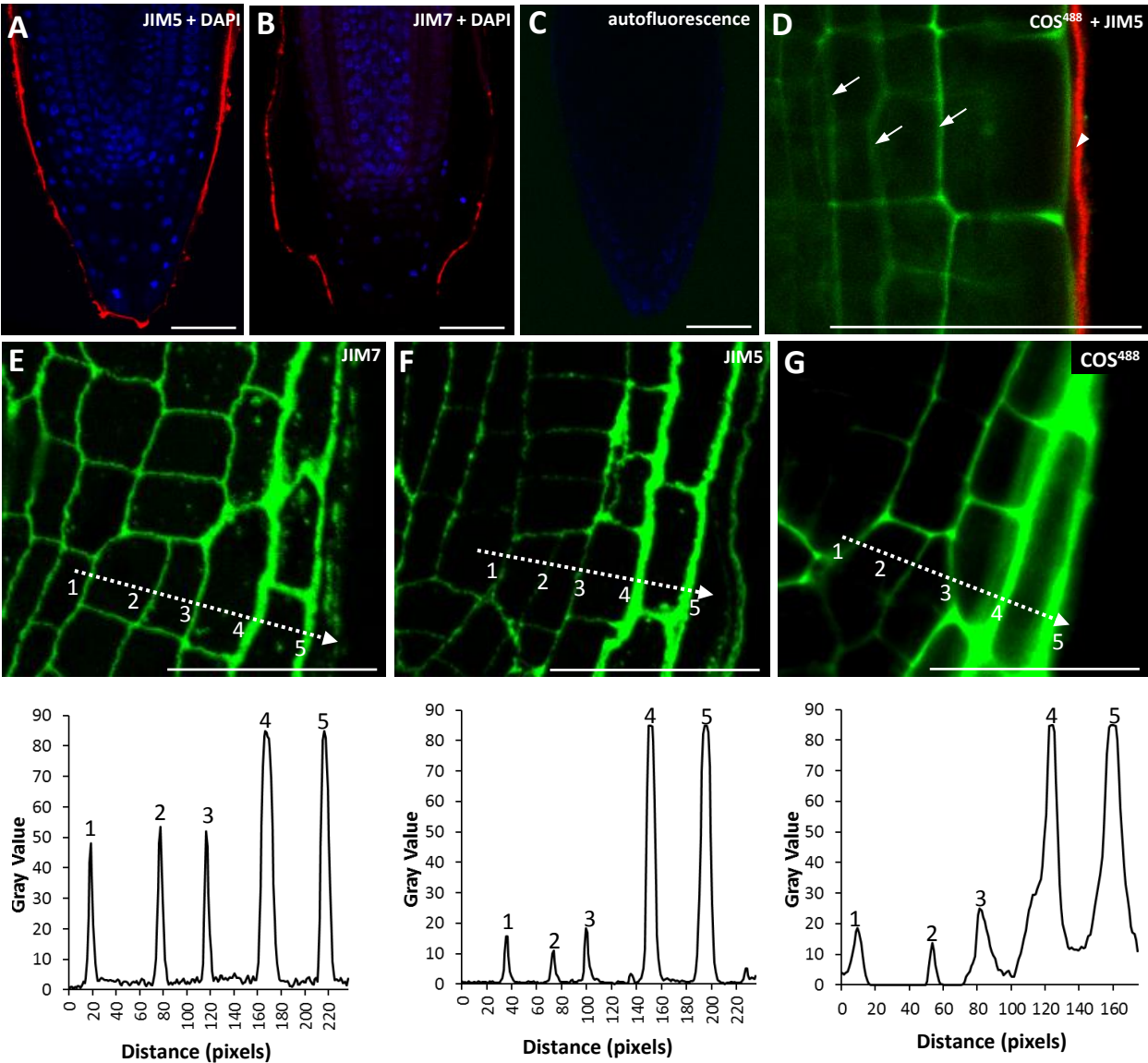


**Fig. S4. Analyses of root tip labelling by mAbs and COS probes.** (A,B) Whole mount labelling of *Arabidopsis* root tips using JIM5 (A) and JIM7 (B). Antibody binding was visualized using with rhodamine-tagged secondary antibody (red). Nuclei are stained with DAPI blue. (C) Control image showing an *Arabidopsis* root tip labeled with secondary antibody only. (D) Dual labelling of a whole unfixed *Arabidopsis* root with COS<sup>488</sup> (green) and the anti-HG monoclonal antibody JIM5 (detected with rhodamine-tagged secondary antibody, red). Note that whilst COS<sup>488</sup> penetrates to the cortical parenchyma (arrows), JIM5 does not penetrate the root (arrowhead). (E-G) Signal intensity analyses of HG labelling in lateral root caps. (E,F) Top panels, sections through resin-embedded root tips labeled by antibodies (E) JIM7 and (F) JIM5. (G) *In vivo* labeling of a whole root tip using COS<sup>488</sup>. Bottom panels: plot profiles showing fluorescence intensities of the regions indicated by the dashed line in the panels above. The positions of the areas producing the peaks are indicated by numbers 1-5. Note that the signal plot profiles indicate a significant increase of JIM5 and COS<sup>488</sup> labelling in the mature root cap layers (4 and 5) compared to antibody JIM7. Scale bars: 10 µm

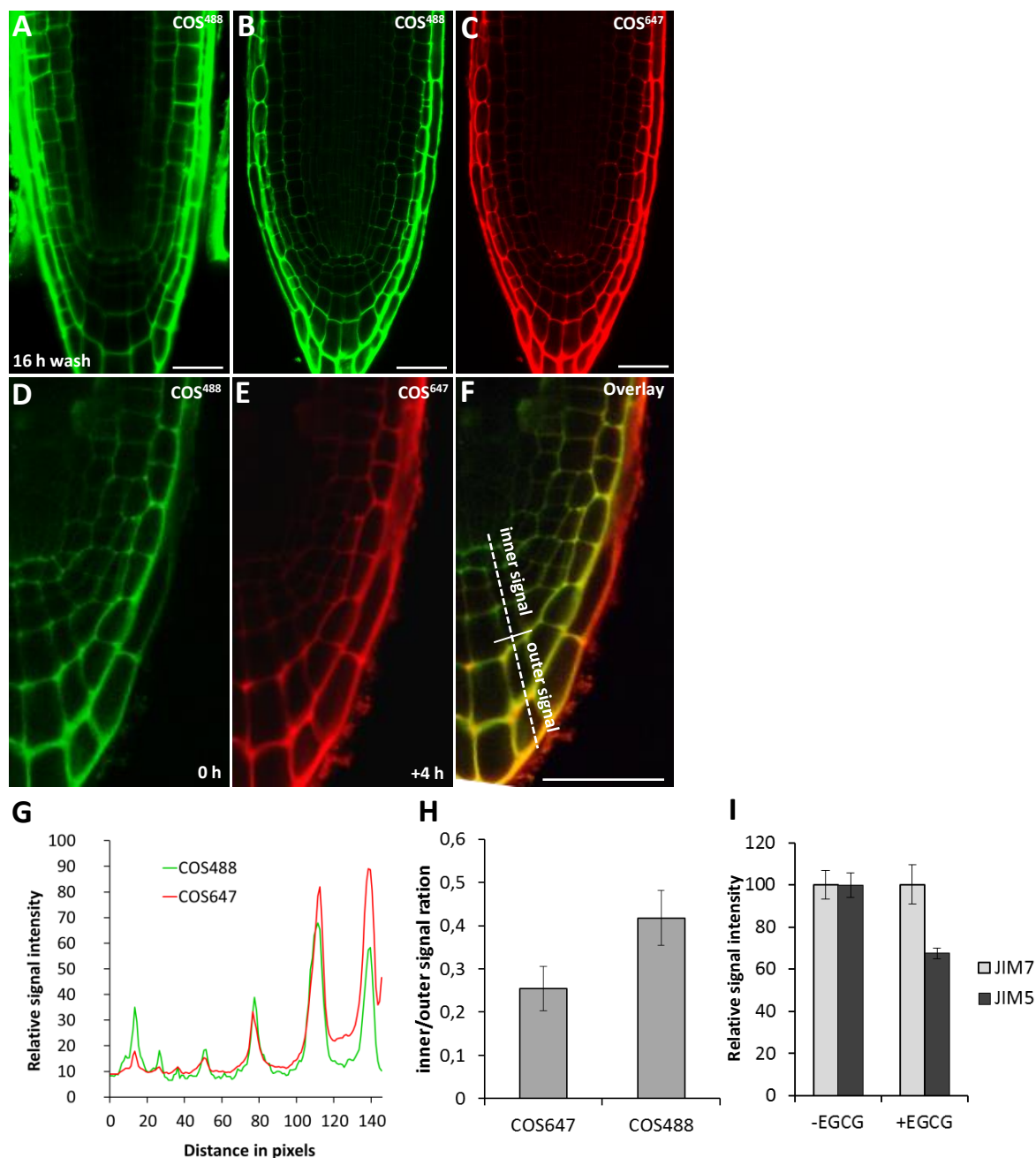


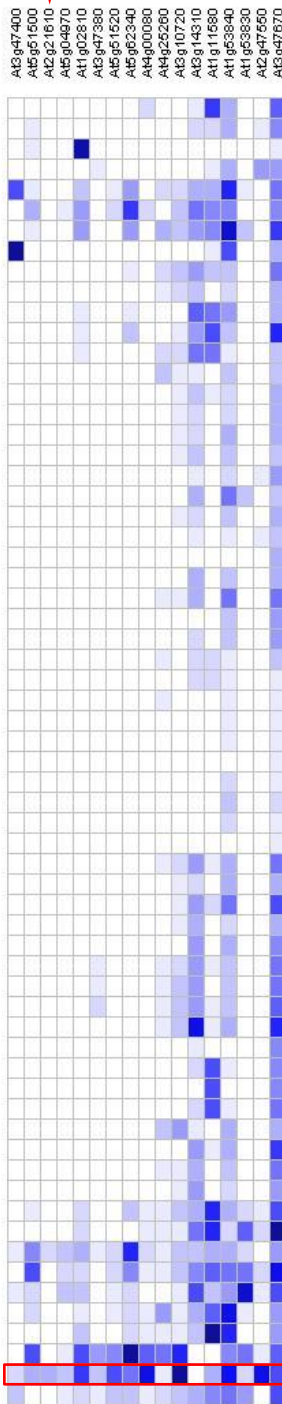
**Fig. S5. Dynamics of HG turn-over in root cap.** (A) Control for the stability of the COS<sup>488</sup> labelling. Fixed roots were stained with COS<sup>488</sup>, washed 3 times and incubated in the labelling buffer for 16h before scanning. No significant wash-out of the probe was observed. (B,C) Comparison of two COS fluorescent variants simultaneously applied to root tips. (B) COS<sup>488</sup> and (C) COS<sup>647</sup> have identical labeling patterns and penetration properties. (D-G) Time lapse labeling of the root tip by two COS variants but in a reverse order as shown in Fig. 3H-K. Seedlings were labelled first using COS<sup>488</sup>, washed and allowed to grow for 4 hours. Seedlings were then re-labelled with COS<sup>647</sup> and washed. The simultaneous scan of (D) COS<sup>488</sup> and (E) COS<sup>647</sup> labelling at the end of the experiment. (F) Overlay image showing the occurrence of newly formed epitopes present in mature layers of the root tip. (G) Plot profile of the dashed line indicated in (F). (H) Quantification of the difference in signal intensities from COS<sup>488</sup> and COS<sup>647</sup> in the 'inner' and 'outer' regions indicated in (F) from 8 root tips. The inner region denotes the first three columella layers and outer region the last two columella layers. Note the higher difference between the two signals in the case of COS<sup>647</sup> (freshly formed epitopes) labelling indicating more signal from the outer region. (I) The effect of EGCG (4 hours at 200  $\mu$ M EGCG) on JIM5 and JIM7 labeling of root tip resin sections. The JIM7 signal was unchanged whilst the JIM5 signal was reduced in roots treated by EGCG. Error bars indicate s.e.m. n=8. Scale bars: 10  $\mu$ m



PME-like

Arabidopsis thaliana

- callus
- cell culture / primary cell
  - sperm cell
  - protoplast
  - root cell
    - root phloem cell
    - root cortex cell
    - root xylem cell
- seedling
  - cotyledons
  - hypocotyl
  - radicle
  - imbibed seed
  - shoot apical meristem
- inflorescence
  - flower
    - carpel
      - ovary
      - stigma
    - petal
    - sepal
    - stamen
      - pollen
      - abscission zone
  - pedicel
- silique
  - replum
- seed
  - embryo
  - endosperm
    - micropylar endosperm
    - peripheral endosperm
    - chalazal endosperm
  - testa (seed coat)
    - general seed coat
    - chalazal seed coat
  - suspensor
- stem
  - developing meristemoidone
- node
- shoot apex
- cauline leaf

- rosette
- juvenile leaf
- adult leaf
- petiole
- senescent leaf
- hypocotyl
  - xylem
  - cork
- leaf primordia
- stem
- axillary bud
- axillary shoot
- roots
- lateral root
- root tip
  - elongation zone
  - root hair zone
  - endodermis
  - endodermis+cortex
  - epid. atrichoblasts
  - lateral root cap
  - stele


PMEI-like

- callus
- cell culture / primary cell
- sperm cell
- seedling
- cotyledons
- hypocotyl
- radicle
- imbibed seed
- inflorescence
- flower
- carpel
- ovary
- stigma
- petal
- sepal
- stamen
- pollen
- abscission zone
- pedicel
- silique
- seed
- embryo
- endosperm
- micropylar endosperm
- peripheral endosperm
- chalazal endosperm
- testa (seed coat)
- general seed coat
- chalazal seed coat
- suspensor
- stem
- node
- shoot apex
- cauline leaf
- rosette
- juvenile leaf
- adult leaf
- petiole
- senescent leaf
- hypocotyl
- xylem
- cork
- leaf primordia
- stem
- roots
- lateral root
- root hair zone
- root tip
- elongation zone
- endodermis
- endodermis+cortex
- epid. atrichoblasts
- lateral root cap
- stele



**Fig. S6. *In silico* expression analyses of PME- and PME-like genes.** Microarray data of PME-like and PME-like genes expressed in *Arabidopsis* root tip from public database (<https://www.genevestigator.com>). Only those with significant expression in root tips are shown. The expression in the root cap is highlighted by red outline. The root cap specific genes analyzed by GUS reporter constructs are indicated by red arrowheads.

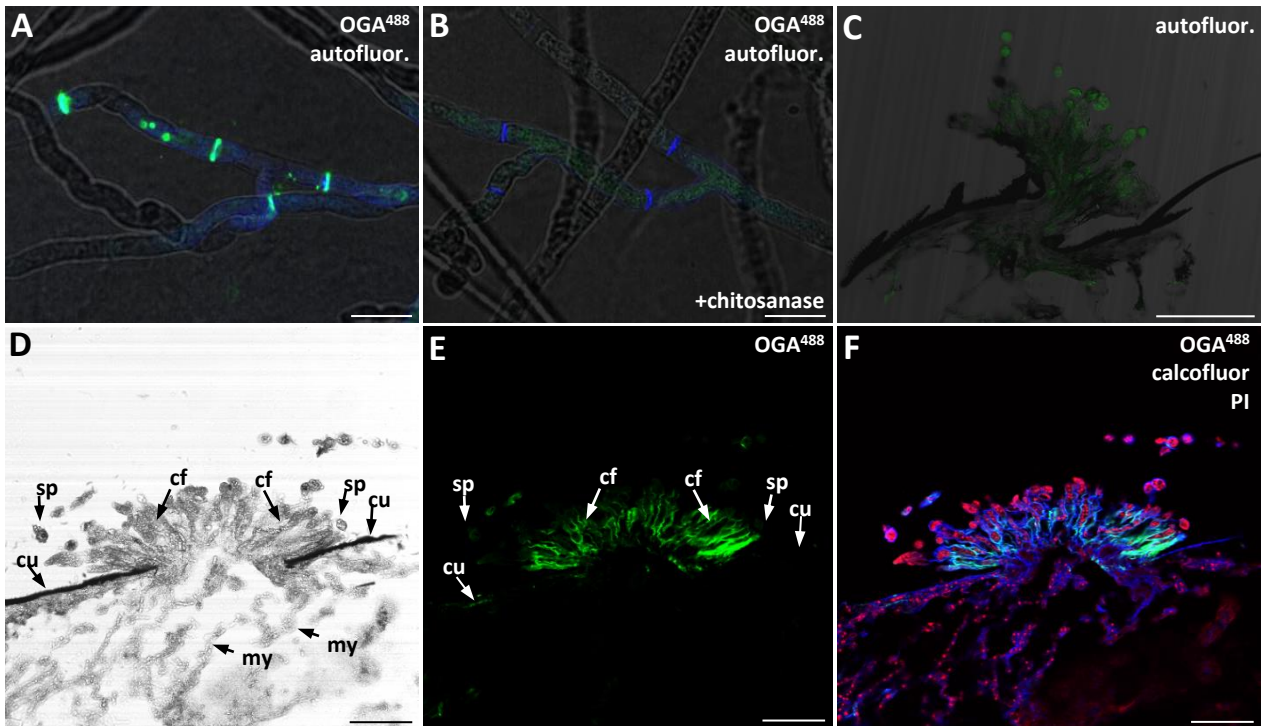


**Fig. S7. Microscopy labelling controls for OGA<sup>488</sup> in fungi.** (A,B) Chitosanase treatment removes the OGA<sup>488</sup> signal (green) in *Neurospora crassa*. Images are overlays with bright field and autofluorescence (blue). (A) Labeling of *N. crassa* mycelium by OGA<sup>488</sup>. (B) Labeling by OGA<sup>488</sup> after chitosanase treatment showing decrease in signal. (C) Control image of unlabeled *E. scizhophorae*. (D) Bright field image of a section through *M. domestica* abdomen infected with *E. scizhophorae*. Conidiophores (cf) and spores (sp) can be seen emerging through the membrane between two cuticle (cu) plates. Hyphae in the mycelia (my) can be seen inside the abdomen. (E) Image shows the same section as in (D) labelled with OGA<sup>488</sup> (green) to reveal chitosan. Note that conidiophores are strongly labelled but not the mycelia or spores. (F) Image showing the same section as in (D) but triple labelled with OGA<sup>488</sup> (green), calcofluor (blue) to reveal chitin and propidium iodide (red) to show nucleic acids. Scale bars: 10  $\mu$ m

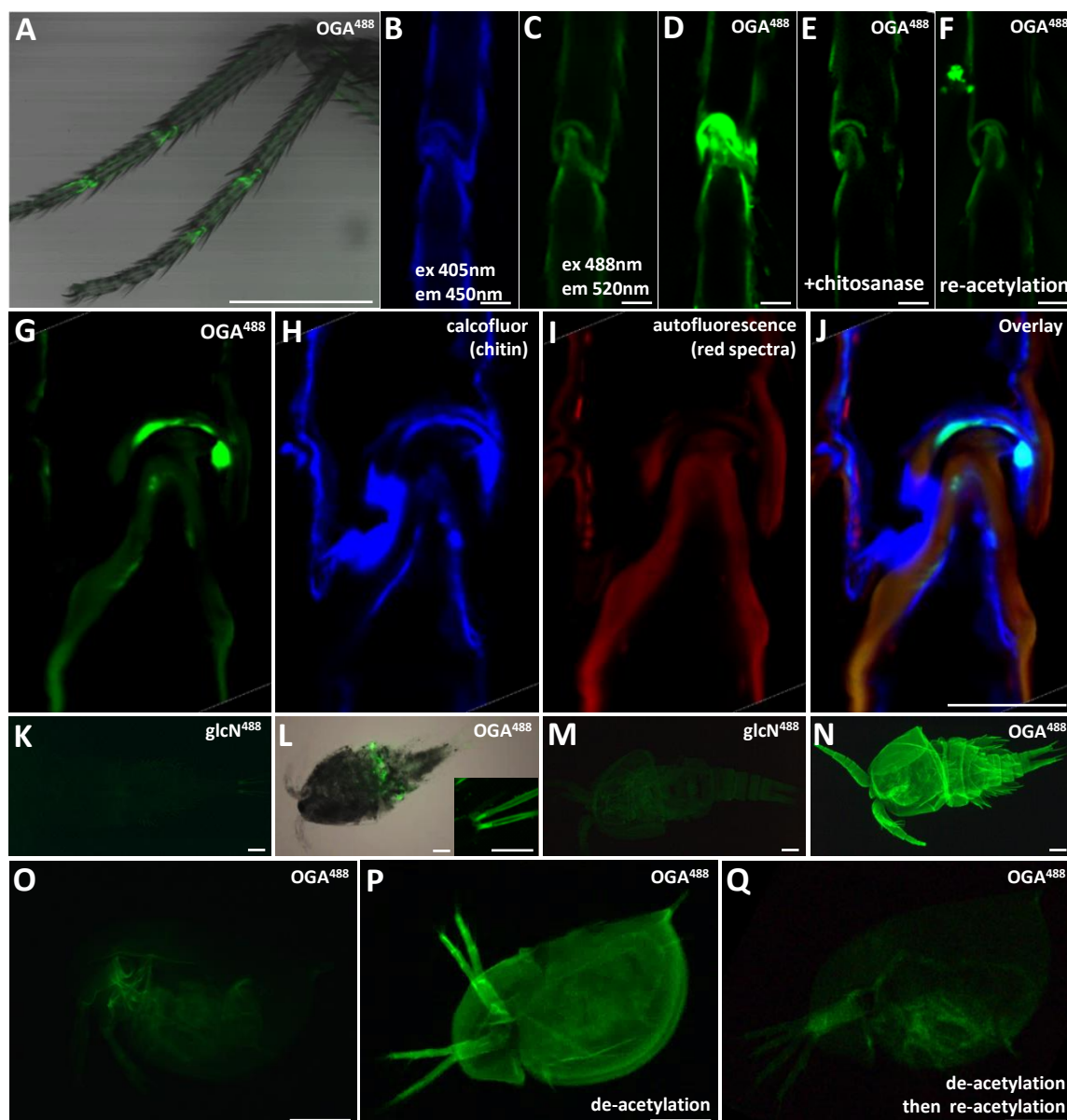


**Fig. S8. Microscopy labelling controls for OGA<sup>488</sup> in arthropods.** (A) Labeling of a whole *Drosophila* leg using OGA<sup>488</sup>. Note the labelling in the tarsal joints. (B-F) Labeling controls for OGA<sup>488</sup> in *Drosophila* joints. (B) Unlabeled control with excitation at 305 nm and emission at 450 nm. (C) Unlabeled control with excitation at 488 nm and emission at 520 nm. (D) Labeling with OGA<sup>488</sup>. Note the strong labelling in the tarsal joint. (E) Chitosanase treatment and (F) chemical re-acetylation of NaOH-treated samples severely decreases OGA<sup>488</sup> binding. (G-J) Labeling of thin resin sections of *Drosophila* tarsal joints. (G) OGA<sup>488</sup> signal. (H) Calcofluor labelling of chitin. (I) Autofluorescence signal with excitation at 555 nm and emission at 620 nm. (J) Overlay of the three channels from (G), (H) and (I). Note the partial co-localization of OGA<sup>488</sup> and calcofluor labelling. (K-N) Labeling of *Cyclops* sp. (K,L) Labelling of untreated *Cyclops* sp. with (K) control conjugate glucosamine<sup>488</sup> and (L) OGA<sup>488</sup>. The picture is an overlay of bright field and the 488 nm channel. Note the central region and the tail labelling (inset). (M, N) Labelling of *Cyclops* sp. after pre-treatment by 5M sodium hydroxide at 99 °C for 1 hour (chemical de-acetylation) by (M) control glucosamine<sup>488</sup> and (N) OGA<sup>488</sup>. The whole exoskeleton containing chemically de-acetylated chitin is visible. (O-R) Labeling of *Daphnia pulex* acetylation control. (O) Labeling of the untreated *Daphnia*. (P) Labeling of chemically de-acetylated *Daphnia*. The whole exoskeleton is visible. (Q) When de-acetylated *Daphnia* was again chemically re-acetylated no signal is visible after OGA<sup>488</sup> labelling. Scale bars: 10 µm for B-J; 100 µm for A and K-Q.